RESEARCH ARTICLE

A GCN1-independent activator of the kinase GCN2

JiaYi Zhu[1†], Giulia Emanuelli[1†], Glenn Robert Masson[2], Vanessa Vinciauskaite[2], Henriette Willems[3], Peiqiao Cai[1], Andrew Lim[3], Christopher Alan Brown[3], David Winpenny[3], Murray Clarke[4], Rebecca Gilley[5], Fergus Preston[6], Jordan CJ Wilson[7], Aldo Bader[7], Taufiq Rahman[8], Joseph E Chambers[1], John Skidmore[3], Nicholas W Morrell[4,9], Stefan J Marciniak[1,4,9]*

[1]Cambridge Institute for Medical Research (CIMR), University of Cambridge, Cambridge, United Kingdom; [2]Division of Cancer Research, School of Medicine, Ninewells Hospital, Dundee, United Kingdom; [3]The ALBORADA Drug Discovery Institute, University of Cambridge, Cambridge, United Kingdom; [4]Department of Medicine, University of Cambridge, Cambridge, United Kingdom; [5]Signalling Programme, The Babraham Institute, Babraham Research Campus, Cambridge, United Kingdom; [6]Domainex Ltd, Churchill Building, Chesterford Research Park, Saffron Walden, United Kingdom; [7]Cancer Research UK Cambridge Institute, University of Cambridge, Cambridge, United Kingdom; [8]Department of Pharmacology, University of Cambridge, Cambridge, United Kingdom; [9]Royal Papworth Hospital NHS Foundation Trust, Cambridge, United Kingdom

***For correspondence:** sjm20@cam.ac.uk

[†]These authors contributed equally to this work

Competing interest: See page 19

Funding: See page 19

Preprint posted
03 July 2025
Sent for Review
31 July 2025
Reviewed preprint v1
26 September 2025
Reviewed preprint v2
10 August 2026
Version of Record
27 October 2026

Reviewing Editor: Julien Roche, Iowa State University, United States

© Copyright Zhu, Emanuelli *et al*. This article is distributed under the terms of the Creative Commons Attribution License, which permits unrestricted use and redistribution provided that the original author and source are credited.

eLife Assessment

This **important** study presents a cell-based screen for small-molecule activators of GCN2, an eIF2α kinase that regulates the Integrated Stress Response under diverse stress conditions. The authors identify a compound as a potent GCN2 activator with GCN1-independent activity under the tested conditions, providing a new pharmacological tool for probing GCN2 regulation. The revised manuscript provides **compelling** support for the central conclusions through a clearer description of the screening workflow, extended kinetic analyses, and demonstration that the identified compound causes a GCN2-dependent reduction in protein synthesis.

Abstract Mutations of *EIF2AK4*, which encodes the eIF2α kinase GCN2, cause a severe inherited form of pulmonary hypertension called pulmonary veno-occlusive disease (PVOD). Some pathogenic variants of GCN2 are amenable to pharmacological reactivation by low concentrations of ATP pocket-binding inhibitors. Kinase inhibition at modestly elevated concentrations limits the clinical utility of these drugs against PVOD. We therefore performed an in cellulo chemical screen for GCN2 activators and identified three structurally distinct compounds with low micromolar stimulatory activities. Unlike previously described GCN2 activators, one of these molecules activated GCN2 independently of GCN1. Modelling supported by structure activity screens suggested it binds within the ATP pocket of GCN2, but unlike existing ligands does not protrude inward into the allosteric pocket or outward into the solvent. This overcomes a key requirement of other GCN2 activators.

Introduction

Phosphorylation of eukaryotic translation initiation factor 2 alpha (eIF2α) mediates the response to a variety of stresses by regulating translation, metabolism, and cell survival (**Harding et al., 2003**; **Emanuelli et al., 2020**). In yeast, GCN2 is the sole eIF2α kinase and triggers the General Control Response to the accumulation of uncharged tRNA and to ribosome stalling (**Gupta and Hinnebusch, 2023**; **Wu et al., 2020**). Gene duplication gave rise to a family of eIF2α kinases in multicellular organisms linking eIF2α phosphorylation to a variety of other stresses. HRI (EIF2AK1) is activated by haem deficiency, oxidative stress, and mitochondrial dysfunction (**Wu et al., 2024**; **Zhu et al., 2022**; **Chakrabarty et al., 2024**), PKR (EIF2AK2) responds to cytosolic double stranded RNA during viral infections, while PERK (EIF2AK3) is activated by endoplasmic reticulum (ER) stress (**Emanuelli et al., 2020**). Mutations affecting these kinases have been linked to the development of disease and so their manipulation by small molecules is being pursued as a means to develop therapies (**Emanuelli et al., 2020**; **Marciniak et al., 2022**; **Carlson et al., 2023**; **Fujimoto et al., 2019**; **Szaruga et al., 2023**).

The eIF2 complex recruits initiator methionyl-tRNA to ribosomes commencing protein synthesis (**Emanuelli et al., 2020**). This requires eIF2 to bind GTP, which is subsequently hydrolysed. Bound GTP is replenished by the guanine nucleotide exchange factor (GEF) eIF2B (**Hinnebusch and Lorsch, 2012**), but phosphorylated p-eIF2α binds avidly to eIF2B inhibiting its GEF activity (**Matts et al., 1983**). When levels of eIF2-GTP-tRNA-Met subsequently fall, most translation is disfavoured, but some transcripts are translated more efficiently owing to the presence of upstream open reading frames within their 5′ untranslated regions (5′UTRs) (**Harding et al., 2003**; **Lu et al., 2004**). ATF4 and CHOP are transcription factors upregulated in this manner during stress to induce genes of the integrated stress response (ISR) (**Harding et al., 2003**; **Emanuelli et al., 2020**; **Lu et al., 2004**). Eventually, PPP1R15A (also called GADD34), itself an ISR target, dephosphorylates p-eIF2α to restore the basal state (**Novoa et al., 2001**; **Marciniak et al., 2004**).

GCN2 is comprised of five domains—RWD, pseudokinase, kinase, HisRS-like, and C-terminal—and exists constitutively as a homodimer (**Emanuelli et al., 2024**; **Masson, 2019**). Its kinase activity is stimulated when the RWD domain interacts with colliding ribosomes via the cofactor GCN1 (**Garcia-Barrio et al., 2000**; **Kubota et al., 2000**; **Sattlegger and Hinnebusch, 2000**) or when the HisRS domain interacts with deacylated tRNAs (**Wek et al., 1995**; **Dong et al., 2000**). Direct interaction between GCN2 and the ribosome P-stalk can also mediate GCN2 activation during ribosome stalling (**Harding et al., 2019**; **Inglis et al., 2019**).

Mutations of *EIF2AK4*, which encodes GCN2, cause the aggressive subtypes of familial pulmonary hypertension, pulmonary veno-occlusive disease (PVOD), and pulmonary capillary haemangiomatosis (**Emanuelli et al., 2020**; **Emanuelli et al., 2024**). Some pathogenic alleles generate hypomorphic variants of GCN2 that we and others have shown can be activated by small molecule inhibitors that bind to the GCN2 ATP pocket, for example neratinib and GCN2iB (**Carlson et al., 2023**; **Szaruga et al., 2023**; **Tang et al., 2022**). Type 1 inhibitors bind the ATP pocket of the kinase in its active conformation (DFG-Asp-in, αC-helix-in), while Type 2 inhibitors bind the inactive conformation (DFG-out, αC-helix-out) (**Roskoski, 2016**). Type 1.5 inhibitors, by contrast, bind an intermediate conformation (DFG-Asp-in, αC-helix-out). Several kinase inhibitors classified as Type 1 or 1.5 with respect to their canonical targets can activate GCN2 at low concentrations while inhibiting it at higher concentrations; however, their binding mode to GCN2 remains undefined (**Carlson et al., 2023**; **Szaruga et al., 2023**; **Tang et al., 2022**). GCN2iB is a relatively selective Type 1.5 inhibitor of GCN2 that activates the kinase at submicromolar concentrations (**Carlson et al., 2023**; **Emanuelli et al., 2024**). It is hypothesised that drug-induced stabilisation of one GCN2 protomer within a dimer is propagated to the second protomer to cause its activation (**Szaruga et al., 2023**; **Neill et al., 2024**). Several inhibitors of other kinases that are in clinical use or development as anticancer agents activate GCN2 in a GCN1-dependent manner, which may contribute to their therapeutic efficacy (**Tang et al., 2022**; **Drainas et al., 2024**; **Tjeerdsma et al., 2025**; **Wilson et al., 2025**). For this reason, GCN2 activators are being sought as potential anticancer drugs.

The complexity of GCN2 activation, involving direct and indirect detection of amino acid deprivation and ribosome stalling, has hampered efforts to reconstitute GCN2 function in vitro (**Solorio-Kirpichyan et al., 2024**; **Bou-Nader et al., 2024**; **Yin et al., 2024**). We therefore performed a cell-based chemical screen for GCN2-dependent activators of the ISR, followed by in vitro validation using orthogonal approaches. In doing so, we identified three novel, structurally distinct GCN2

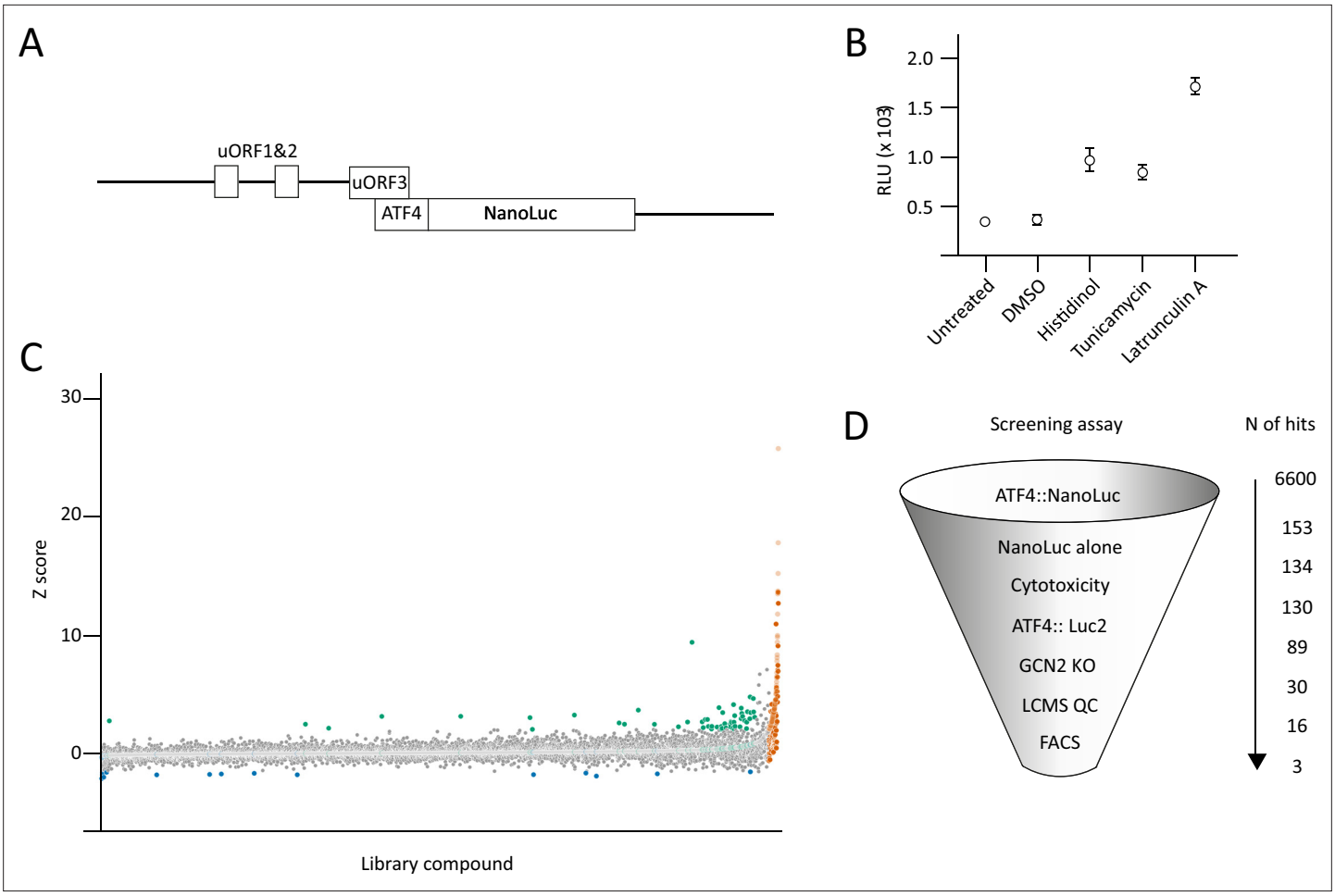


Figure 1. Chemical screen of novel GCN2-specific ISR-activating molecules. (**A**) Schematic of ATF4::NanoLuc reporter, exploiting the upstream open reading frames (uORFs). Short uORFs 1, 2, and 3 precede the ATF4 translation start site, with uORF3 overlapping the ATF4 coding sequence, but out-of-frame. During the ISR, skipping of uORF3 leads to increased translation initiation at the ATF4 initiator AUG. (**B**) Relative Light Unit (RLU) of ATF4 signal in CHO stable cell-line overexpressing ATF4::NanoLuc treated with 1 mM histidinol, 2.5 µg/ml tunicamycin, or 1 µM latrunculin A (n = 3 biological repeats; ± SEM). (**C**) Chemical screen of 6461 small molecules tested with CHO stable cell-line overexpressing ATF4::NanoLuc. The molecules were treated alone or with submaximal ISR activation with 0.3 mM histidinol. All molecules were displayed along the x-axis based on their Z-score of relative reporter signal when treated with compound alone (pale symbols). Z-score for treatment with compound and histidinol is also plotted at the same x-axis position (dark symbols). Molecules with Z-score >3 (i.e. over 3 standard deviations from the mean reporter signal) were identified as hits: ISR activator in orange and ISR augmenter (exaggerating ISR activation by histidinol) in green. (**D**) Pipeline of molecule short-listing, primary screening using CHO ATF4::NanoLuc reporter (153 hits), NanoLuc alone control (134 hits), selection based on cytotoxicity (130 hits), orthogonal CHO ATF4::FLuc reporter (89 hits), and subsequent GCN2 specificity in GCN2 null reporter cells (30 hits) and compound quality control via liquid chromatography–mass spectrometry (LC–MS; 16 hits), finally validation by GCN2-specific FACS to a short list of three compounds.

The online version of this article includes the following source data for figure 1:

Source data 1. Results of chemical screen.

activators. Notably, one of these, designated compound 20, activates GCN2 in a GCN1-independent manner.

Results

Chemical screen for GCN2 activators

We generated clonal Chinese Hamster Ovary (CHO) cell lines expressing an ATF4::NanoLuc reporter comprising the 5′UTR of human ATF4 mRNA fused to NanoLuc luciferase (***Figure 1A***; ***Emanuelli et al., 2024***). Activation of the ISR could be detected as bioluminescence in response to ISR activators histidinol, tunicamycin, and latrunculin A (***Figure 1B***). Histidinol activates GCN2 by inhibiting histidyl-tRNA

synthetase, leading to the accumulation of uncharged $tRNA^{His}$. This uncharged tRNA binds to GCN2, relieving its autoinhibition and activating the kinase (**Grummt and Grummt, 1976**). Latrunculin A sequesters G-actin, thereby inhibiting PPP1R15A activity (**Oliveira et al., 2024**; **Chambers et al., 2015**). Tunicamycin inhibits protein glycosylation in the ER, resulting in activation of PERK (**Harding et al., 1999**). A high-throughput screen of the BioAscent library of 123,222 drug-like compounds performed by the ALBORADA Drug Discovery Institute yielded two pools of potential ISR inhibitors and activators. Compounds were classified based on *Z*-score thresholds derived from the primary screen, with activators defined as those with *Z*-score >3. An initial analysis of 121,000 compounds, excluding plates failing quality control, identified 6521 activators, of which 6461 overlapped with the subset selected for follow-up screening. Minor discrepancies were restricted to compounds absent from the analysed dataset (e.g. originating from failed plates) or those with *Z*-scores close to the threshold (3–3.02), consistent with limited analytical variation. Using this approach, we assembled a subset of 6461 compounds enriched for potential ISR activators and screened these in 384-well format at 10 µM for 16 hr. To increase sensitivity, screens were performed with test compound alone or combined with the half-maximal effective concentration (EC_{50}) of histidinol. This submaximal concentration was used to allow detection of compounds that enhance ISR signalling when GCN2 is partially activated. This yielded 153 compounds that activated the reporter at least three standard deviations above baseline (*Z*-score >3) (**Figure 1C**).

The pipeline used to filter hit compounds is illustrated in **Figure 1D**. Counter screens were performed against constitutively expressed Nanoluc, to exclude trivial activators of luminescent proteins, leaving 134 hits. Cytotoxicity assays excluded immediately toxic compounds, leaving 130. While primary screening was performed in ATF4-Nanoluc lines for maximal sensitivity, hits were subsequently re-tested in a second CHO ATF4::luc2 reporter line as a more stringent orthogonal assay to prioritise robust ISR activators. Of the 130 hits identified in the sensitive Nanoluc screen and passing early toxicity assessment, 89 were confirmed in the luc2 assay, consistent with enrichment for higher-amplitude ISR activators under more stringent detection conditions. In subsequent mechanistic studies, the ATF4-Nanoluc reporter was again used to take advantage of its higher sensitivity and simpler assay format for multi-condition comparisons.

GCN2-deficient ATF4::NanoLuc CHO reporter cells were generated by introducing the reporter into *Eif2ak4*$^{-/-}$ CHO cells (**Harding et al., 2019**). Thirty compounds were selected based on GCN2 dependency, where stimulation was lost in GCN2 null cells. Liquid chromatography–mass spectrometry verified compound purity and quality leaving 16 lead compounds of high confidence from the original library stocks.

Orthogonal secondary screen

Although hits were prioritised for GCN2 dependence, we performed an additional orthogonal screen to exclude compounds that activate the ISR indirectly via ER stress, which converges on the same downstream outputs. The ISR can be activated in isolation or in combination with other stress signalling pathways, for example as part of the unfolded protein response (UPR) to ER stress (**Emanuelli et al., 2020**). To distinguish between inducers of ER stress and selective activators of the ISR, we used dual-reporter CHO cells that express a fluorescent ISR reporter (CHOP::GFP) and a reporter of IRE1 activity (XBP1::Turquoise) (**Sekine et al., 2016**). Histidinol served as a positive control for ISR activation via GCN2, while tunicamycin was used to induce ER stress and activate the UPR. *Eif2ak4*$^{-/-}$ CHO cells were used to assess GCN2 dependence, while *Ppp1r15a*$^{-/-}$ cells, which are impaired in the dephosphorylation of eIF2α, were used to amplify the effects of ISR activation. Histidinol selectively activated the CHOP::GFP ISR reporter in wild-type and *Ppp1r15a*$^{-/-}$ cells, but not in GCN2 deleted cells, validating this system (**Figure 2A**). Activation of the ISR by tunicamycin was exaggerated in the *Ppp1r15a*$^{-/-}$ cells owing to their defective dephosphorylation of eIF2α (wild-type vs *Ppp1r15a*$^{-/-}$, $p < 0.05$). Tunicamycin activated both the CHOP::GFP and XBP1::Turquoise reporter in all three genotypes.

The 16 lead compounds were next examined both in the presence and absence of a submaximal concentration of histidinol. Using this orthogonal approach, three compounds were found to be GCN2 selective activators of the ISR (**Figure 2B, C**). Those which induced ER stress or showed minimal GCN2 dependence are not shown. Reporter activation was measured by fluorescence activated cell sorting (FACS) after 18 hr of treatment with 30 µM compound 18, 20 µM compound 20, and 7.5 µM compound 21. The three GCN2 selective activators included compound 18, *N-(4-{[(furan-2-yl)methyl]*

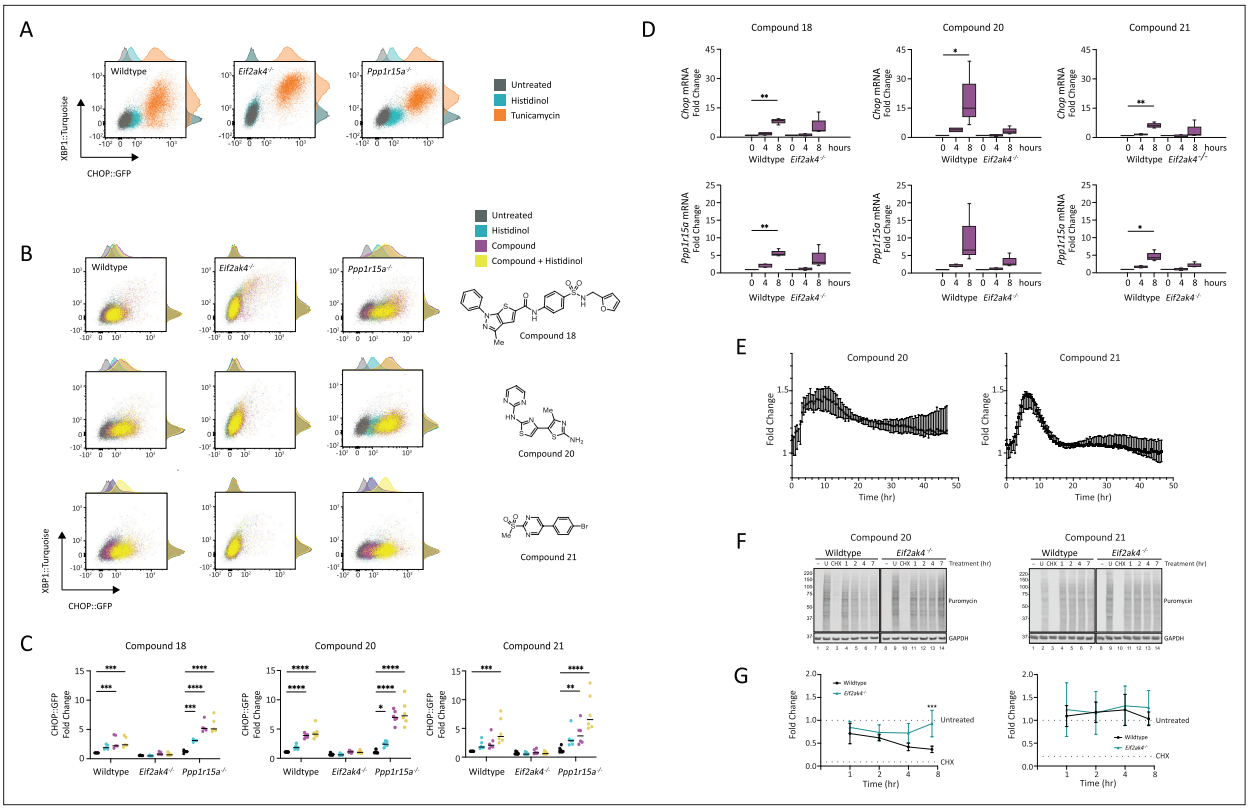


Figure 2. Shortlist and characterisation of top hits. Representative dot plot of flow cytometry data in CHO CHOP::GFP and XBP1::Turquoise dual-reporter wild-type, *Eif2ak4Δ*, and *Ppp1r15aΔ* cells under 18-hr treatment of 0.75 mM histidinol (blue), 2 µg/ml tunicamycin (orange), and untreated control (grey) (*n* = 2 biological repeats). Bi-exponential display was used for the plots. The *x*-axis represents fluorescence signals at 530 nm for GFP (CHOP reporter) and *y*-axis represents fluorescence signals at 450 nm for turquoise (XBP1/IRE1 reporter). (**B**) Representative bi-exponential displayed dot plot of flow cytometry data in CHO CHOP::GFP and XBP1::Turquoise dual-reporter wild-type, *Eif2ak4Δ*, and *Ppp1r15aΔ* cells under 18-hr treatment of 30 µM compound 18, 20 µM compound 20, and 7.5 µM compound 21 alone (magenta) or in combination with 0.75 mM histidinol (yellow) (*n* = 6 biological repeats). Histidinol alone is shown in blue and untreated in grey. The *x*-axis represents fluorescence signals at 530 nm for GFP (CHOP reporter) and *y*-axis represents fluorescence signals at 450 nm for turquoise (XBP1/IRE1 reporter). Structures of compounds 18, 20, and 21 shown on the right. (**C**) Quantification of B (*n* = 6 biological repeats); Two-way ANOVA with Tukey's multiple comparisons test was performed and the CHOP-GFP signals (530 nm) in different treatment groups were compared. *p ≤ 0.05, **p ≤ 0.01, ***p ≤ 0.001, ****p ≤ 0.0001. (**D**) Box and whisker plot displaying mRNA fold-change of ISR effector CHOP and PPP1R15A after 4- and 8-hr treatment of 30 µM compound 18, 10 µM compound 20, and 10 µM compound 21 as detected by quantitative real-time PCR (qPCR; *n* = 3 biological repeats; ± SEM), two-way ANOVA was performed, *p ≤ 0.05, **p ≤ 0.01. (**E**) Wild-type CHO cells stably expressing the ATF4::nanoLuc-PEST reporter were treated with Nano-Glo and either (left) 13 µM compound 20 or (right) 13 µM compound 21. Median bioluminescence (fold-change normalised to DMSO control) ± 95% confidence. Representative experiment (*n* = 4 technical repeats). (**F**) Representative immunoblots of lysates from wild-type or *Eif2ak4*$^{-/-}$ CHO cells treated with 10 µM compound 20 or 7.5 µM compound 21 for the indicated times. Immediately before harvesting, cells were treated with 10 µg/ml puromycin to label newly synthesised polypeptides. '-' indicates cells not incubated with puromycin. 'U' cells were treated with puromycin but without test compound. 'CHX' represents the cycloheximide control (100 µg/ml). Molecular size in kDa. (**G**) Quantification of puromycinylated proteins normalised to GAPDH. Mean ± SEM. CHO WT (black) and *Eif2ak4*$^{-/-}$ cells turquoise. *N* = 4 independent experiments. Two-way ANOVA with Šídák's multiple comparisons test; ***p ≤ 0.001.

The online version of this article includes the following source data for figure 2:

Source data 1. Uncropped immunoblots for ***Figure 2F***.

Source data 2. Original western blots of ***Figure 2F***.

Source data 3. Numerical data used to generate ***Figure 2***.

sulfamoyl}phenyl)-3-methyl-1-phenyl-1H-thieno[2,3c]pyrazole-5-carboxamide, containing a furan and two phenyl rings; compound 20, *4'-methyl-N~2~-2-pyrimidinyl-4,5'-bi-1,3-thiazole-2,2'-diamine*, containing two aminothiazoles; and compound 21, *5-(4-bromophenyl)-2-(methylsulfonyl)pyrimidine* (***Figure 2B***).

Larger quantities of compound 18 were then purchased from TimTec, USA (compound ST51216373); compound 20 was synthesised by ChemBridge, USA (compound 5935953); and compound 21 was

purchased from Specs, Netherlands (compound AC-907/25005415). After validating their effects using the assays described above, we next confirmed activation of the ISR by these compounds at the transcriptional level at 4 and 8 hr. CHO cells were treated with 30 μM of compound 18 or 10 μM of compound 20 or 21 for 4 and 8 hr and expression of the ISR target genes *Chop* and *Ppp1r15a* was measured using quantitative real-time PCR (qPCR; ***Figure 2D***). All three induced ISR gene expression, with compound 20 eliciting the strongest response.

Studies with compound 18 were limited by poor aqueous solubility; therefore, time-course analyses focused on compounds 20 and 21. To assess ISR activation over an extended period, live-cell luciferase measurements were performed using CHO cells stably expressing an ATF4::Nanoluc-PEST reporter. Both compounds elicited maximal reporter activation between 6 and 8 hr (***Figure 2E***). Compound 20, but not 21, induced a significant GCN2-dependent reduction in mRNA translation, as measured by puromycin incorporation, with a progressive effect observed up to 7 hr (***Figure 2F, G***).

Cell-line differences in GCN2 activator potencies

Neratinib is an ATP-competitive pan-HER kinase inhibitor used clinically in the treatment of breast cancer (***Guo et al., 2023***). Recent studies have shown that the sensitivity of glioblastoma cells to neratinib is dependent on GCN2, with GCN2 activation observed at submicromolar concentrations but inhibition at higher concentrations (***Tang et al., 2022***). We reproduced this biphasic activation of the ISR reporter in human cervical carcinoma HeLa cells and hamster CHO cells, recording EC_{50} values for activation of 269 nM (95% CI 218–322 nM) and 690 nM (95% CI 634–772 nM), respectively (***Figure 3A***). Disruption of the *EIF2AK4* gene by CRISPR/Cas9 (*EIF2AK4*$^{-/-}$) in HeLa cells abrogated ISR activation confirming the effect to be mediated by GCN2 (***Figure 3A***, middle panel).

In CHO cells, compound 18 was the least potent with an EC_{50} of greater than 30 μM without obvious inhibition up to 100 μM (***Figure 3B***). Notably, compound 18 failed to activate the ISR measurably in either HeLa cells or human embryonic kidney 293T cells (***Figure 3C***). Compound 20 activated the ISR in CHO cells in a biphasic manner with an EC_{50} of 4.8 μM (95% CI 4.0–5.6 μM) (***Figure 3B***). It was active in 293T cells though with a lower potency, EC_{50} of 17 μM, but was inactive in HeLa cells (***Figure 3C***). Compound 21 also showed biphasic activation of the ISR in CHO cells with an EC_{50} of 5.0 μM (95% CI 3.9–6.5 μM) (***Figure 3B***). Weak activation was observed in 293T cells, but none was seen in HeLa cells (***Figure 3C***). To benchmark ISR activation in these models, each cell type was treated with 3 mM histidinol (***Figure 3D***). Reporter activation was most robust in CHO cells, followed by 293T cells, then HeLa cells.

GCN2iB, a potent inhibitor of GCN2, abolished histidinol-induced activation of the ATF4::NanoLuc ISR reporter in CHO cells confirming this to be GCN2 mediated (***Figure 3E***). Supporting a role for GCN2 in mediating the compounds' effects, GCN2iB substantially reduced ISR reporter expression by each, though this effect was only partial at concentrations of compound 20 above 10 μM (***Figure 3D***). This might indicate GCN2-independent effects or an ability to partially outcompete GCN2iB for binding at higher concentrations.

We went on to examine downstream cellular consequences of GCN2 activation in multiple models. While compounds did not induce detectable ISR signalling in HCT116 or COS-7 cells under the conditions tested, induction of PPP1R15A was observed in Mesobank T12 primary mesothelioma cells, indicating context-dependent biological responses. Moreover, in contrast to GCN2iB (***Emanuelli et al., 2024***), the current compounds did not activate disease-associated GCN2 variants linked to PVOD (data not shown).

Compound 20 activates GCN2 in a GCN1-independent manner

GCN1 mediates the interaction between stalled ribosomes and GCN2 (***Sattlegger and Hinnebusch, 2000***; ***Pochopien et al., 2021***). Histidinol is a competitive inhibitor of the histidyl-tRNA synthetase that depletes the cell of charged histidyl-tRNA, thus causing ribosome stalling and activation of the ISR in a GCN1-dependent manner (***Pochopien et al., 2021***; ***Hansen et al., 1972***; ***Snieckute et al., 2022***). Using GCN1-deficient human 293T cells transiently expressing the ATF4::NanoLuc reporter, we confirmed that activation of the ISR by histidinol requires GCN1 (***Figure 4A***). Low concentrations of GCN2iB (5–70 nM) had minimal effect on ISR reporter activation, while neratinib robustly triggered the ISR. The stimulatory effects of neratinib were significantly attenuated in GCN1-deficient cells consistent with the observation that GCN1 knockout renders astrocytoma cells resistant to neratinib

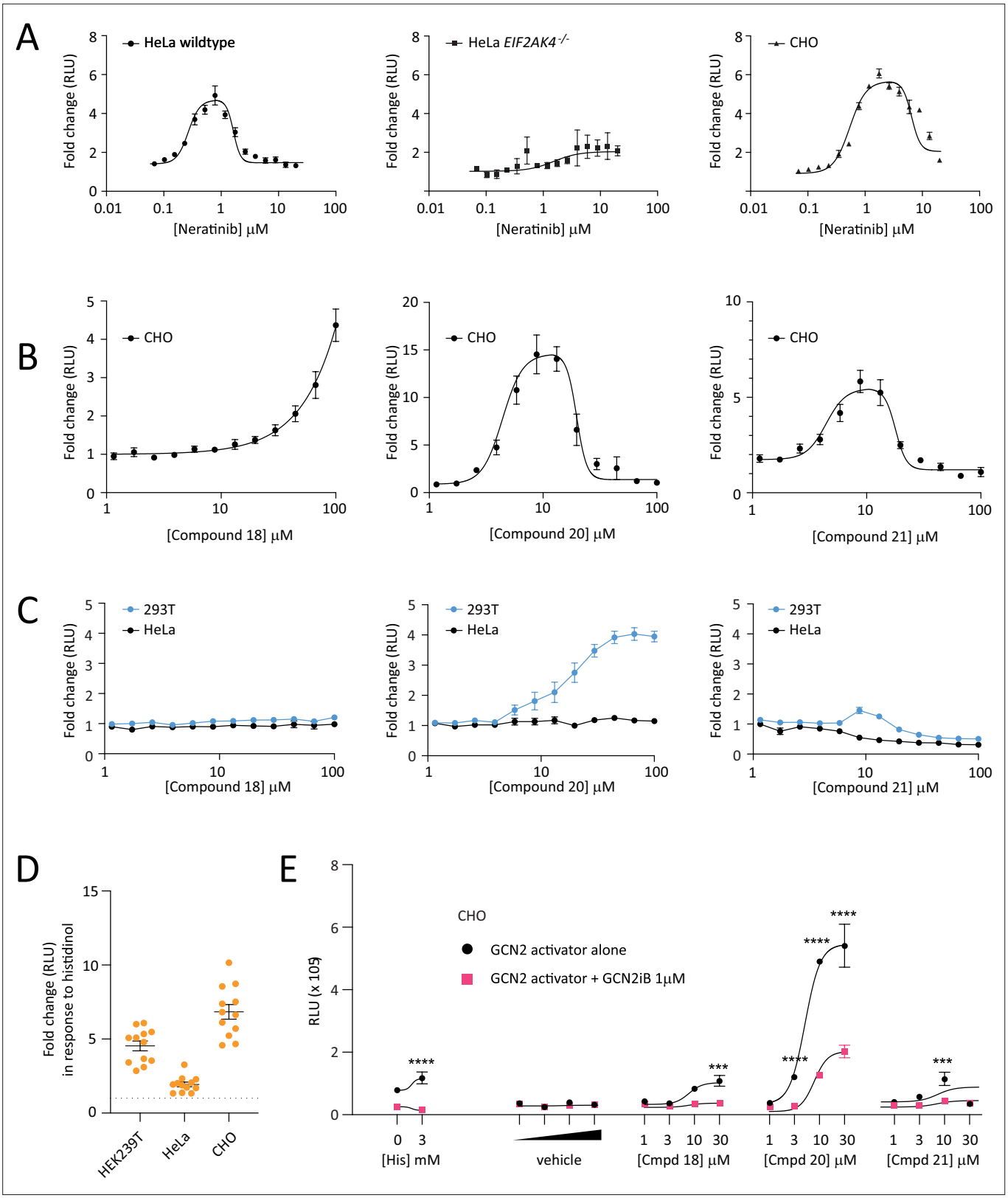


Figure 3. Compounds 18, 20, and 21 display cell type-specific differences in ISR activation. (**A**) Normalised dose-dependent fold-change in ATF4 expression by neratinib in HeLa WT, HeLa *EIF2AK4Δ*, and CHO WT ATF4::NanoLuc reporter cells after 16-hr treatment (n = 3 biological repeats; mean ± SEM). DMSO was used as vehicle. (**B**) Normalised dose-dependent fold-change in ATF4 expression by compounds 18, 20, and 21 in CHO WT ATF4::NanoLuc reporter cells after 16-hr treatment (n = 3 biological repeats; mean ± SEM). EC_{50} was estimated using 4-parameter non-linear regression.

Figure 3 continued on next page

Figure 3 continued

DMSO treatment was used as vehicle. (**C**) Normalised dose-dependent fold-change in ATF4 expression by compounds 18, 20, and 21 in HeLa (black) and 293T (blue) WT cells transiently transfected with ATF4::NanoLuc reporter after 16-hr treatment (n = 3 biological repeats; ± SEM). DMSO treatment was used as vehicle. (**D**) Fold-change of ATF4::NanoLuc reporter signal in HEK293T, HeLa and CHO cells transiently transfected with reporter and treated for 20 hr with 3 mM histidinol. Fold-change calculated relative to vehicle control (n = 3 biological repeats; mean ± SEM). (**E**) Relative Light Unit (RLU) of ATF4 signal in CHO WT ATF4::NanoLuc reporter cells treated with 1, 3, 10, and 30 µM Compounds 18, 20, and 21 alone (black) or in combination with 1 µM GCN2iB (pink) for 18 hr (n = 3 biological repeats; ± SEM). 0.01, 0.03, 0.1, and 0.3% DMSO served as vehicle and 3 mM histidinol as positive control. Two-way ANOVA was performed; ***p ≤ 0.001, ****p ≤ 0.0001.

The online version of this article includes the following source data for figure 3:

Source data 1. Data of cell type differences.

(***Tang et al., 2022***). By contrast, activation of the ISR by compound 20, chosen for having the largest effect size in 293T cells, did not require GCN1 to activate the ISR reporter (***Figure 4A***). Indeed, loss of GCN1 modestly increased ISR activation at the highest concentration of compound 20 suggesting a mode of action independent of ribosome stalling. To gain confidence in this observation, we inactivated the *Gcn1* gene in CHO cells by CRISPR/Cas9. Neratinib-induced activation of the ATF4::NanoLuc ISR reporter was lost in GCN1-deficient CHO cells; however, ISR activation by compound 20 was completely insensitive to loss of GCN1 (***Figure 4B***).

No systematic assessment of GCN1 dependence has previously been performed for GCN2 activating drugs. We therefore proceeded to test a panel of ten additional kinase inhibitors that had been reported to activate GCN2 (***Carlson et al., 2023***; ***Szaruga et al., 2023***; ***Tang et al., 2022***). Our panel included examples of multi-targeted tyrosine kinase inhibitors (dovitinib, sunitinib), RAF inhibitors (LY3009120, dabrafenib), inhibitors of the Wee1 kinase involved in G2 cell cycle checkpoint (WEE1-IN-4, AZD1775, Debio0123), an inhibitor of the Heat Shock Factor 1 pathway (NXP800), and EGFR inhibitors (erlotinib and gefitinib) (***Carlson et al., 2023***; ***Szaruga et al., 2023***; ***Tang et al., 2022***; ***Wilson et al., 2025***; ***Gilley et al., 2024***; ***Pacey et al., 2024***; ***Ill et al., 2024***). In all cases, a marked reduction in GCN2 activation by the drugs was observed in GCN1-deficient cells (***Figure 4C***). Most of these molecules failed to activate the ISR in the absence of GCN1 (sunitinib, NXP800, dovitinib, AZD1775, dabrafenib, gefitinib, LY3009120), while for three drugs weak activation of the ISR was seen at higher concentrations (WEE1-IN-4, Debio 0123, erlotinib). None showed the dramatic GCN1 independence observed for compound 20 in unstressed cells.

To further assess the mechanism of compound-induced ISR activation, we evaluated reporter responses in GCN2-deleted cells (***Figure 4D***). Several compounds, including sunitinib, NXP800, WEE1-in-4, Debio0123, gefitinib, and erlotinib, showed reduced reporter activity in GCN2-deficient cells, consistent with GCN2-dependent activation. In contrast, dovitinib, AZD1775 and dabrafenib produced weaker or inconclusive responses even in the paired wild-type lines, limiting analysis. These data allow us to distinguish compounds consistent with direct or GCN2-dependent activation from those more likely to induce ISR indirectly through cellular stress upstream of GCN2. These findings support a distinction between compounds that activate the ISR through GCN2-dependent mechanisms and those that likely act indirectly via alternative stress pathways.

ATP-competitive interaction with the GCN2 kinase domain

Existing activators of GCN2 have been shown to interact with the ATP-binding pocket (***Carlson et al., 2023***; ***Szaruga et al., 2023***; ***Tang et al., 2022***). We therefore used a bioluminescence resonance energy transfer (BRET)-based assay to examine the interaction of the three lead compounds with the kinase domain of GCN2 in cells. Briefly, the N-terminal portion of human GCN2 kinase domain fused to NanoLuc luciferase was expressed in either CHO or 293T cells. These were then treated with an ATP-binding pocket tracer. In this system, energy transfer is proportional to tracer binding to the NanoLuc-tagged kinase domain, and so interactions of other molecules that displace the tracer reduce the BRET ratio (***Figure 5A***; ***Robers et al., 2021***). In both CHO and 293T cells, GCN2iB efficiently suppressed the BRET ratio thus validating the system (***Figure 5B***). All three lead compounds significantly reduced the BRET ratio, though unlike GCN2iB, compounds 18 and 20 were noticeably more effective in CHO than in 293T cells. Although compound 21 suppressed BRET in both cell types, its effect was less dramatic in CHO cells compared to compounds 18 and 20. The concentrations

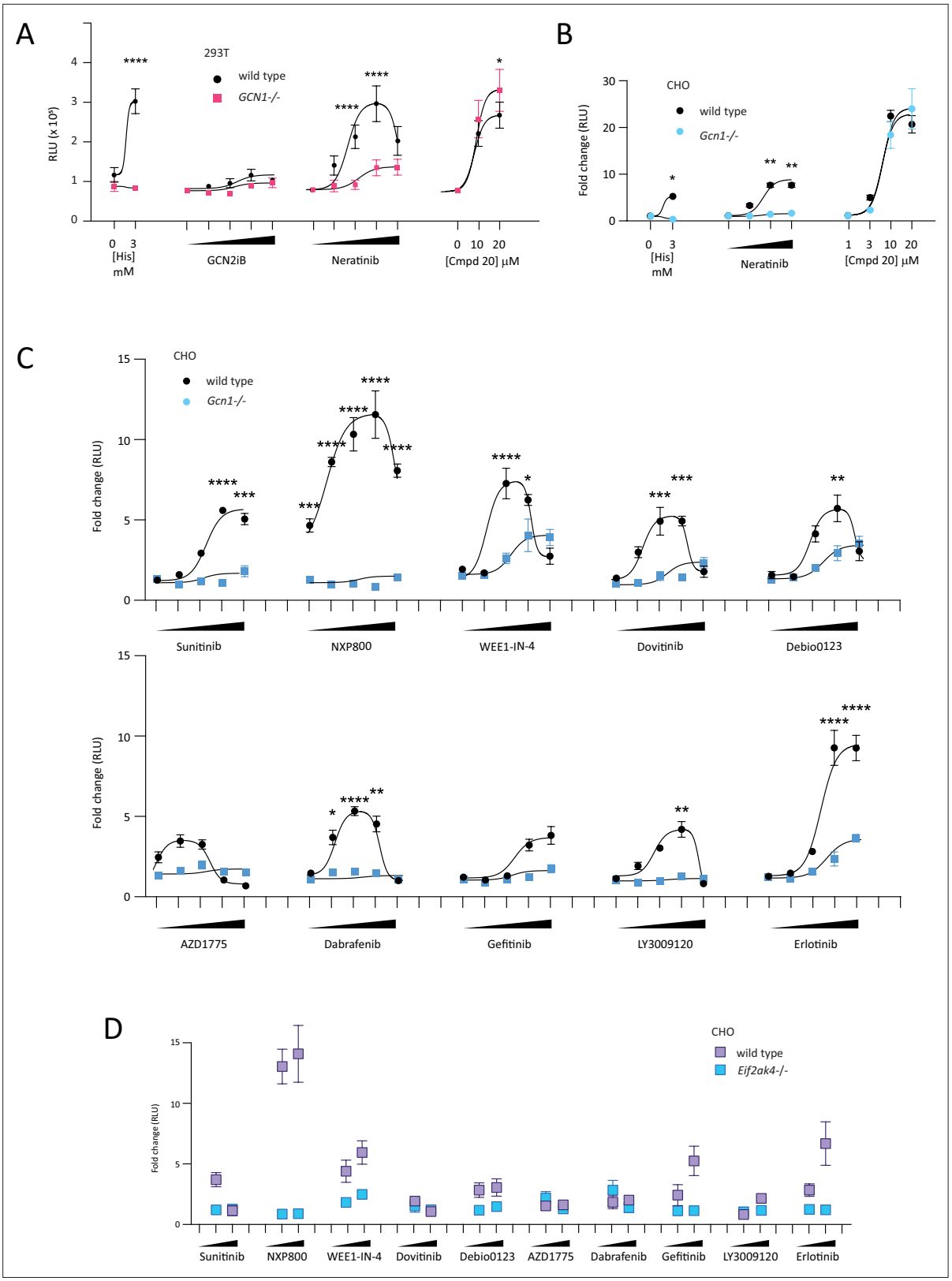


Figure 4. Compound 20 displays GCN1 independence. (**A**) Relative Light Unit (RLU) of ATF4 signal in 293T WT (black) and GCN1Δ (magenta) cells transiently transfected with ATF4::NanoLuc reporter for 16-hr treatment with compound 20 (10 and 20 µM), GCN2iB (5, 10, 35, and 75 nM), and neratinib (75, 200, 500, and 1000 nM) (*n* = 3 biological repeats; ± SEM). Two-way ANOVA was performed; *p ≤ 0.05, **p ≤ 0.01, ***p ≤ 0.001, ****p ≤ 0.0001. (**B**) Normalised fold-change in ATF4 signal in CHO WT (black) and *Gcn1−/−* (blue) ATF4::NanoLuc reporter cells for 18-hr treatment with compound

Figure 4 continued on next page

Figure 4 continued

20 (1, 3, 10, and 30 μM) and neratinib (75, 200, and 500 nM) (*n* = 3 biological repeats; ± SEM). Two-way ANOVA; *p ≤ 0.05, **p ≤ 0.01. (**C**) Normalised fold-change in ATF4 signal in CHO WT (black) and *Gcn1−/−* (blue) ATF4::NanoLuc reporter cells treated for 19 hr with a panel of ATP-competitive kinase inhibitors reported to activate GCN2 (0.1, 0.3, 1, 3, and 10 μM) (*n* = 3–9 biological repeats; mean ± SEM). Two-way ANOVA was performed; *p ≤ 0.05, **p ≤ 0.01, ***p ≤ 0.001, ****p ≤ 0.0001. (**D**) Normalised fold-change in ATF4 signal in CHO WT (purple) and Gcn2−/− (blue) ATF4::NanoLuc reporter cells treated for 19 hr with a panel of ATP-competitive kinase inhibitors reported to activate GCN2 (at 1 and 3 μM, sunitinib used at 3 and 10 μM, AZD1175 used at 0.3 and 1 μM, gefitinib and erlotinib used at 3 and 10 μM). DMSO was used as vehicle control (*n* = 3 biological repeats; mean ± SEM).

The online version of this article includes the following source data for figure 4:

Source data 1. Compound 20 displays GCN1 independence.

required to detect target engagement in NanoBRET assays did not directly mirror those required for ISR activation, reflecting the distinction between ligand binding and downstream pathway output.

To examine further the interaction of compounds 18 and 20 with GCN2's kinase domain, we generated in bacteria a recombinant protein comprising glutathione *S*-transferases (GST) fused to the kinase domain of human GCN2 (residues 585–1005 of NCBI reference Sequence NP_001013725.2). GST was chosen both to facilitate protein purification and to enhance dimerisation of the kinase domain in order to cause autophosphorylation and constitutive activation. When incubated in vitro with increasing concentrations of ATP and a fixed quantity of His6-tagged bacterially expressed eIF2αN-terminal domain (***Marciniak et al., 2006***), GST–GCN2 kinase domain phosphorylated its substrate on serine51, as detected by immunoblotting (***Figure 5C***). Neratinib dose-dependently inhibited eIF2αphosphorylation (***Figure 5D***, lanes 1–5). The lack of activation by neratinib likely reflected the requirement for autoinhibitory domains of GCN2 to observe this effect. Therefore, in this system inhibition of eIF2α kinase activity was used as a surrogate for target engagement. Compounds 18 and 20 also inhibited eIF2αphosphorylation, while compound 21 appeared inactive in this assay (***Figure 5D***). Compounds 18 and 20 altered the apparent kinetic parameters of GCN2, including an increase in the observed V_{max}; however, these data do not allow assignment of a specific inhibition modality (***Figure 5E, F***).

To test the ability of compound 20 to activate full-length GCN2, we next generated full-length human GCN2 (uniprot ID: Q9P2K8) through baculoviral expression using an N-terminal twin StrepII tag. Despite exerting only a modest effect on GCN2 autophosphorylation at T899 within the activation loop, compound 20 robustly triggered the phosphorylation of full-length eIF2αto an even greater extent than purified tRNAs, a known endogenous stimulus of GCN2 activity (***Figure 5G***). Of note, uncharged tRNA produced a modest (~4-fold) activation of GCN2 under these conditions, whereas compound 20 induced substantially greater (~40-fold) activation.

Interaction with other ISR kinases

The eIF2α kinases have a common evolutionary origin and consequently the kinase domains share some structural similarity (***Dalton et al., 2012***). We therefore examined the effect of the compounds on all four eIF2α kinases in vitro. Lower concentrations of ATP (10 μM for GCN2, 0.1 μM for PERK, 0.15 μM for HRI, and 0.1 μM for PKR) were used to accentuate antagonism at the ATP site. This assay was performed at low ATP concentrations to sensitise detection of ATP-competitive inhibition and was not optimised to detect compound-mediated activation of GCN2. Under these conditions, in contrast to ***Figure 5G*** where 100 μM ATP was used, activation of GCN2 is not observed with any of the compounds tested. At low ATP, full length, purified GCN2 was efficiently inhibited by GCN2iB with an IC_{50} of 1.55 nM. None of the screen hits reached 50% inhibition at the highest concentration tested (3 μM) though compound 20 and to a lesser extent 18 appear to cause weak inhibition (***Figure 6A***). Minimal inhibition was observed with the test compounds again purified PERK (***Figure 6B***). The PERK inhibitor GSK2606414 served as a positive control with an expected IC_{50} of 0.66 nM. Weak inhibition of HRI by compounds 18 and 20 was observed but failed to reach 50% (***Figure 6C***). In this system, GCN2iB was found to inhibit purified HRI with an IC_{50} of 2.76 nM, similar to that observed against GCN2. By contrast, both compounds 18 and 20 inhibited PKR in vitro: compound 18 with an IC_{50} of 4.50 μM and compound 20 with an IC_{50} of 3.75 μM (***Figure 6B–D***). GCN2iB inhibited PKR with an IC_{50} of 3.26 μM. Compound 21 was inactive against each of the four eIF2α kinases in this assay.

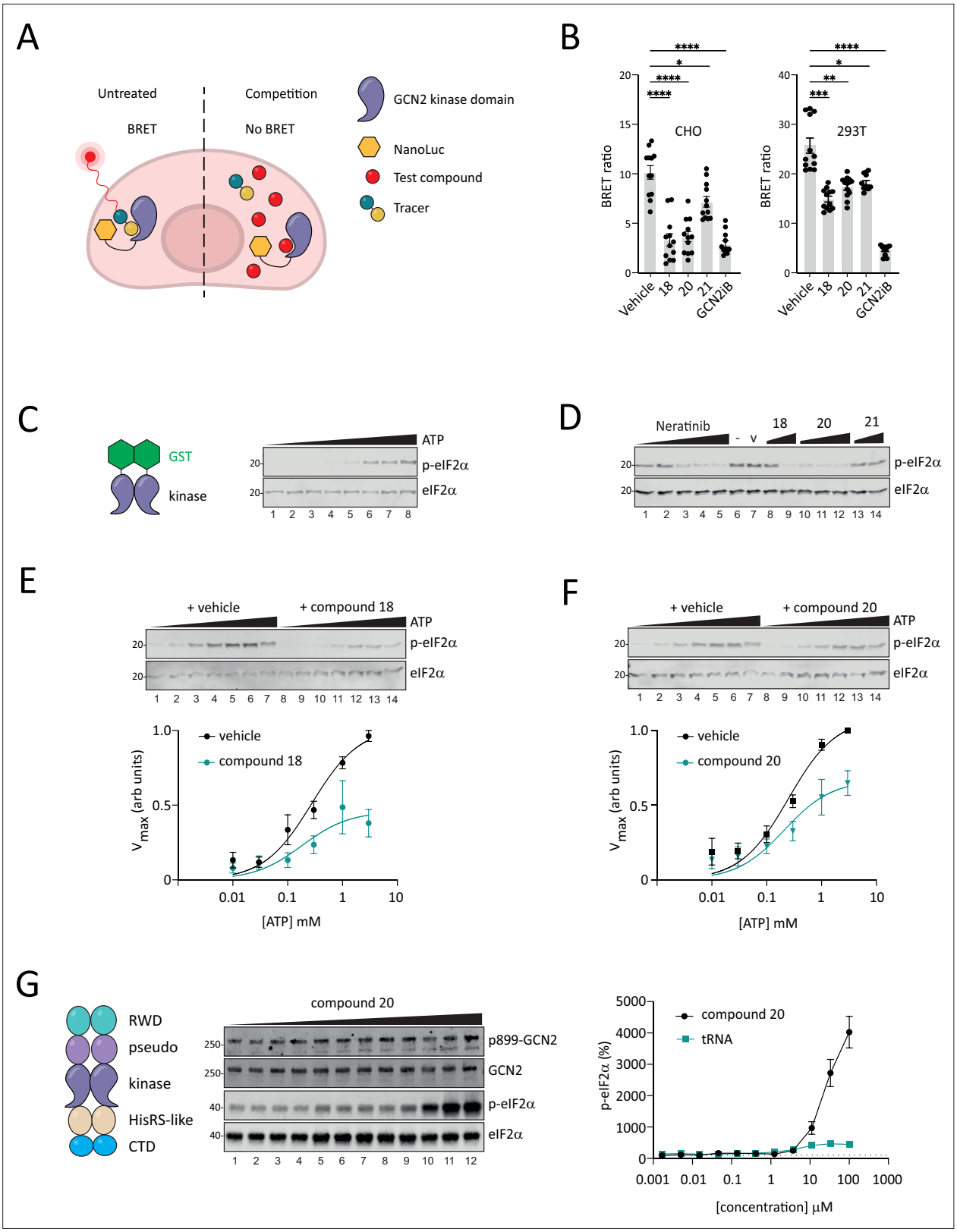


Figure 5. Compounds 18 and 20 directly bind to GCN2 in cellulo and in vitro. (**A**) Illustration of the NanoBRET assay. Left panel displays BRET signal at baseline with tracer binding to GCN2; right panel displays reduced BRET signal due to the addition of a competitive compound that outcompetes the tracer from binding to GCN2. (**B**) BRET ratio in CHO and 293T WT cells with 2-hr treatment of 3% DMSO, 100 μM compounds 18, 20, and 21 or 0.5 μM GCN2iB (n = 3 biological repeats; ± SEM). Two-way ANOVA was performed; *p ≤ 0.05, **p ≤ 0.01, ***p ≤ 0.001, ****p ≤ 0.0001. (**C**) Schematic

Figure 5 continued on next page

Figure 5 continued

of GST–GCN2 fusion protein (residues 585–1005) and representative immunoblot of in vitro kinase assay. Purified GST–GCN2 was incubated with eIF2α-NTD (residues 2–187) using a ramp of ATP concentrations (0, 0.01, 0.03, 0.1, 0.3, 1, 3, and 10 mM) (*n* = 3 biological repeats). Total and serine51 phosphorylated eIF2α were detected. (**D**) Representative immunoblot of in vitro kinase assay showing inhibition of eIF2α-NTD (residues 2–187) phosphorylation. Purified GST–GCN2 and eIF2α-NTD were incubated with neratinib (0.075, 0.68, 6.67, 10, and 20 μM) and compound 18 (100–500 μM), compound 20 (100, 200, and 500 μM), and compound 21 (100–500 μM) (*n* = 3 biological repeats). 5% DMSO was used as vehicle control. Total and serine51 phosphorylated eIF2α were detected. Molecular size in kDa. (**E**) Representative immunoblot of in vitro kinase assay (*n* = 3 biological repeats) showing inhibition of eIF2α-NTD (residues 2–187) phosphorylation by 300 μM compound 18 using a ramp of ATP concentrations (0.01, 0.03, 0.1, 0.3, 1, 3, and 10 mM); 3% DMSO was used as vehicle control. Bottom panel showed Michaelis–Menten kinetics analysis of DMSO control (black) vs compound 18 (green). Molecular size in kDa. (**F**) Representative immunoblot of in vitro kinase assay (*n* = 3 biological repeats) showing inhibition of eIF2α-NTD (residues 2–187) phosphorylation by 100 μM compound 20 using a ramp of ATP concentrations (0.01, 0.03, 0.1, 0.3, 1, 3, and 10 mM); 3% DMSO was used as vehicle control. Bottom panel showed Michaelis–Menten kinetics analysis of DMSO control (black) vs compound 20 (green). Molecular size in kDa. (**G**) Schematic of full-length GCN2 protein and representative immunoblot of in vitro kinase assay. Purified full-length GCN2 was incubated with full-length eIF2a using a ramp of compound 20 or tRNA concentrations (0, 0.001, 0.005, 0.01, 0.05, 0.13, 0.4, 1.2, 3.7, 11, 33, and 100 μM) (*n* = 3 biological repeats). Total and serine51 phosphorylated eIF2a, as well as total and threonine899 phosphorylated GCN2 were detected. On the right showed quantification of serine51 phosphorylated eIF2a with a ramp of tRNA (black) vs compound 20 (green). Molecular size in kDa.

The online version of this article includes the following source data for figure 5:

Source data 1. Uncropped immunoblots for ***Figure 5C–G***.

Source data 2. Orginal western blots of ***Figure 5C–G***.

Source data 3. Compounds 18 and 20 directly bind to GCN2 in cellulo and in vitro.

In silico docking of compounds 18 and 20 to the GCN2 kinase domain and structure–activity relationship analysis

We used the SiteMap module from Schrodinger Suite to identify binding sites based on drug interactions with nearby GCN2 residues. Published crystal structures of the GCN2 kinase domain (see methods) show the ATP-binding pocket comprises a large solvent-exposed region and a buried hydrophobic region that extends beyond the gatekeeper residue (Met802) and towards the αC-helix (***Figure 7***). Compound 18 was predicted to occupy a similar pocket to that of the ligand in the PDB 6N3N crystal structure demonstrating a Type 1.5-binding configuration, characterised by the DFG loop being 'in' and the αC-helix being in the 'out' conformation (***Fujimoto et al., 2019***). The furan motif of compound 18 was predicted to be buried in the allosteric pocket around αC-helix, between gatekeeper Met802 and Leu640 (***Figure 7D***). The compound's sulfone was predicted to interact with Phe867 of the conserved DFG motif. In neratinib, a triad of hydrogen bonding was predicted between the 8-position of the isoquinoline core (Ar–H bond), the amine linker (H bond) and the 2-position of the fluorobenzene ring (Ar–H bond) with Asp866, similar to the predicted interaction between the amide linkage of compound 18 and Asp866 (***Figure 7B***). Both neratinib and compound 18 were also predicted to protrude into the solvent-exposed space (***Figure 7B–E***). However, the interaction of neratinib with Cys805 of the hinge region through the nitrile of isoquinoline core was not present in compound 18.

Due to the metabolic liabilities of furans in medicinal chemistry programmes, we sought to explore the importance of this motif for binding and activity using available structural analogues. Replacement of the sulfonamide furan motif with some benzene derivatives including phenolic (BCC0106222), 2-bromobenzene (BCC0113320), and 3-acetylbenzene (BCC0104214) preserved ISR activation while others (BCC0073242 and BCC0043997) resulted in a loss of activity (***Appendix 1—table 1***). Incorporation of heterocyclic ring systems (BCC0073142 and Z56783036) or modification of solvent-exposed region (Z88478561, Z226209130, and Z11741677) were similarly not tolerated (***Appendix 1—table 1***). However, modifying the furan motif to benzene derivative 2-bromobenzene (BCC0113320) and heterocyclic ring (BCC0077119) preserved GCN2-specific ISR activation.

Unlike compound 18 and neratinib, compound 20 was not predicted to protrude into the allosteric pocket (***Figure 7F, G***). Analogues extending further towards the αC-helix and protruding into the solvent-exposed region were inactive (e.g. Z118606822), suggesting that the small size of compound 20 may be advantageous, fitting into the ATP-binding pocket of GCN2 and facilitating stronger activation (***Appendix 1—table 1***). Hydrogen bond interaction was predicted between the NH_2 of the compound 20 aminothiazole with the carbonyl of the hinge region Cys805. Additional interaction was predicted between the linker NH of compound 20 and backbone carbonyl of Asp866 in the DFG

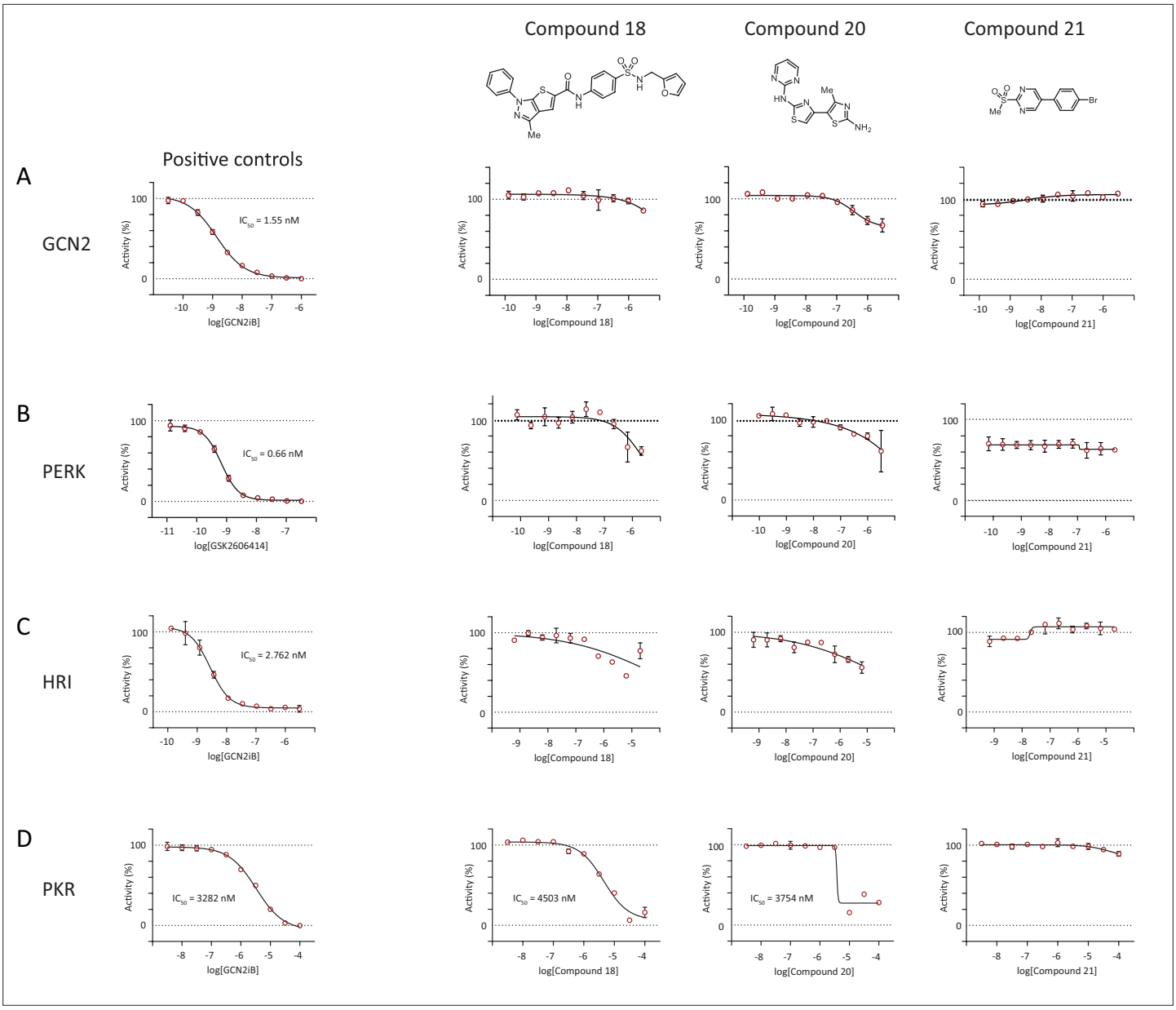


Figure 6. Compound activity across eIF2α kinases using *LanthaScreen* in vitro *kinase activity assay*. Left panels: dose-dependent inhibition of GCN2, PERK, HRI, or PKR with positive control drug GCN2iB or GSK2606414. Right panels: effect of concentration ranges of compounds 18, 20, and 21 in this system revealed weak inhibition of GCN2, HRI, and PKR (n = 2 biological repeats). Low ATP concentrations were used to accentuate inhibition, and this masks the stimulatory effects on GCN2.

The online version of this article includes the following source data for figure 6:

Source data 1. Compound activity across eIF2α kinases using *LanthaScreen* in vitro kinase activity assay.

motif. Such 2-aminopyrimidine rings are present in many kinase ligands (***Jadhav et al., 2021***). Rather than this interacting with hinge region residues, this moiety in compound 20 was predicted to form a pi–cation interaction with Lys619 and a hydrogen bond with DFG Asp866, as has been reported for other ligands of kinase ATP pockets (***Fujimoto et al., 2019***). Replacement of this pyrimidine ring with 2-pyridine analogues (BCC0084738, BCC0079350, and BCC0083923) was well tolerated, likely due to the conserved hydrogen bonding interaction between the pyridine nitrogen and Asp866. Removal of a nitrogen from the ring system, such as BCC0057014, BCC0089519, BCC0084744, and BCC0084833 all resulted in a loss of activity, possibly due to their lack of interaction with Asp866 (***Appendix 1—table 1***). Due to toxicity issues surrounding 3-aminothiazoles, modifications were made to replace

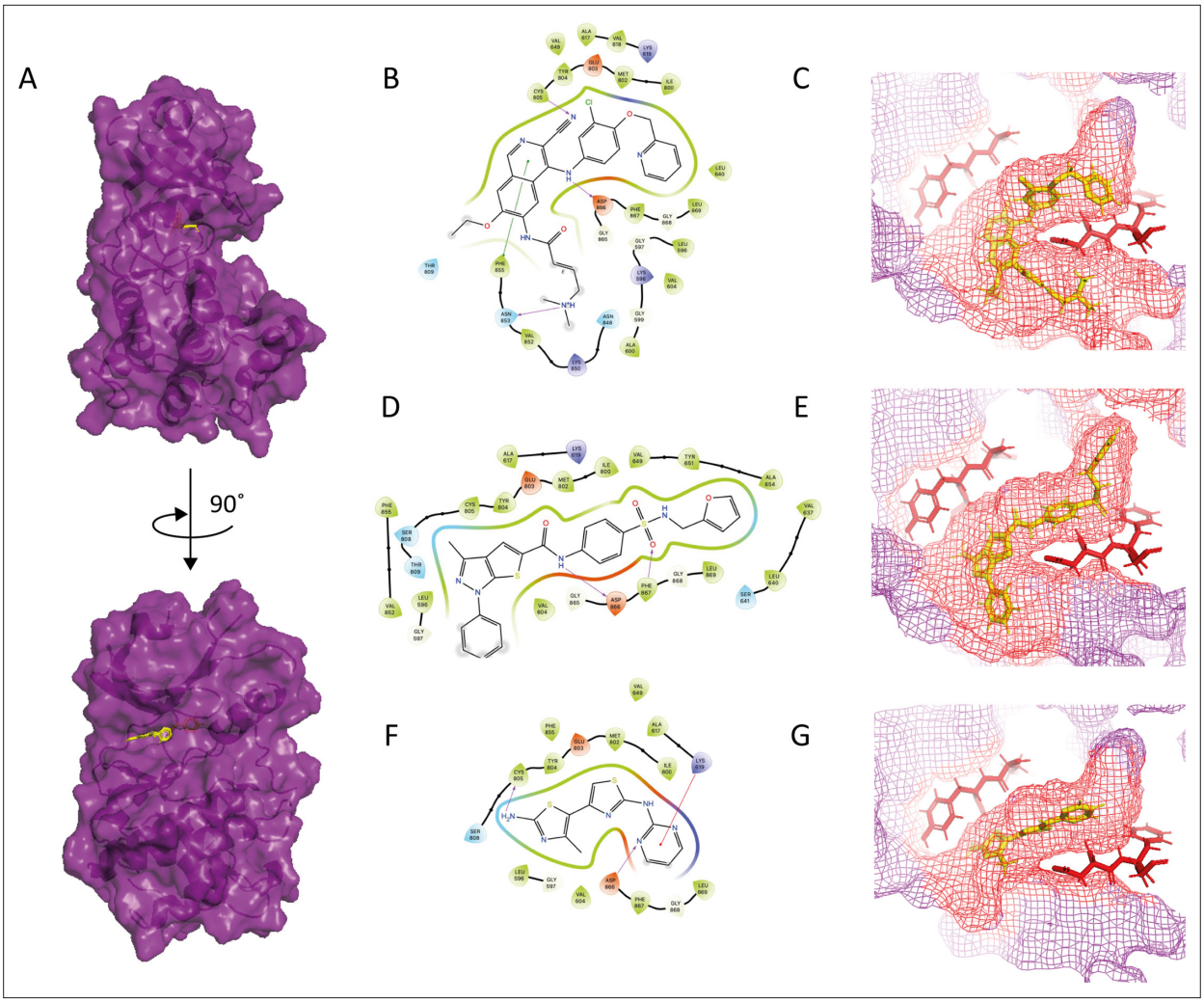


Figure 7. Structural modelling. (**A**) Illustration of GCN2 kinase domain from up (N-terminus) to down (C-terminus) with illustrative ligand (yellow) in ATP-binding pocket. (**B**) 2D ligand interaction diagram of neratinib, (**D**) compound 18, and (**F**) compound 20. Violet, green, and red coloured lining indicate hydrogen bond, *π*–*π*, and cation–*π* interactions, respectively. Polar and hydrophobic residues are highlighted in blue and green, respectively. Mesh representation of the ATP-binding pocket in GCN2 kinase domain was shown with ligand (yellow): (**C**) neratinib, (**E**) compound 18, and (**G**) compound 20. Key residues surrounding the ATP-binding pocket, including the DFG motif (D866–G868) and EYC residues (E803–C805) following the gatekeeper M802 were labelled red. Figures adapted from crystal structure 6N3N.

the terminal thiazole ring system with phenyl derivatives (BCC0080152, BCC0075509, BCC0084830, BCC0057431, and BCC0080200). However, these resulted in a decrease in activity towards GCN2, suggesting that there might be a steric component contributing to activity. Replacing the thiazole with a minimally steric affecting thiophene (BCC0079876) also led to activity loss, possibly due to the twisting of central thiazole ring that impaired hydrogen bonding between pyrimidine nitrogen and Asp866. We were therefore unable to improve upon compound 20's activity but gained valuable structure–activity relationship (SAR) information for future development.

To provide additional context on the developability of the identified compounds, we performed an in silico assessment of key physicochemical and pharmacokinetic properties. Predicted blood–brain barrier (BBB) permeability scores suggested a gradient across compounds, with compound 18 scoring 5.13 (indicative of a high likelihood of central nervous system penetration), compound 20 scoring 4.29 (moderate predicted penetration), and compound 21 scoring 3.35 (lower likelihood of brain exposure), consistent with its greater polarity. Analysis of lipophilicity, reflecting how readily a compound partitions into lipid membranes, showed that compound 18 has relatively balanced properties (*c* log *P* 1.84; log *D* 1.98) but very low aqueous solubility (0.07), which may limit bioavailability. Compound 20 exhibited more moderate lipophilicity alongside improved solubility (0.67), whereas compound

21 was the most lipophilic and the least soluble, indicating a less favourable balance of properties. As expected, solubility decreased with increasing molecular weight and lipophilicity. Taken together, these data indicate that compound 20 achieves the most favourable balance between solubility, lipophilicity, and predicted tissue distribution, consistent with a more drug-like profile and supporting its prioritisation for further development.

Discussion

The ISR plays a critical role for maintaining homeostasis under diverse stress conditions and its disruption results in a variety of disease states (***Emanuelli et al., 2020***). The observation that some pathogenic variants of GCN2 are amenable to pharmacological activation led us to seek novel GCN2 activators. Our chemical screen identified three chemically distinct GCN2 activating molecules, one of which is, to our knowledge, the first to show independence from GCN1 for its activity. This may prove useful as a tool compound for the study of GCN2 in cells and using purified components since it overcomes at least one hurdle to kinase activation.

Recent work suggests that the ATP-competitive modulator GCN2iB can activate GCN2 independently of GCN1 under specific conditions using a GCN2 E26A mutant (***Carlson et al., 2023***). In our hands, we did not observe GCN1-independent activation with GCN2iB at the concentrations tested. This discrepancy may reflect a narrow concentration window for GCN1-independent activation or context-dependent effects of the E26A mutation. These findings raise the possibility that GCN1-independent activation of GCN2 may occur under specific conditions or with distinct classes of compounds.

Compounds 18 and 20 demonstrate weak inhibition of the related kinase PKR. Previous structural analyses have shown the kinase domains of PKR and GCN2 to be highly conserved, particularly at the ATP-binding pocket, which likely contributes to this effect. Indeed, a previous publication reported that other small molecule inhibitors of GCN2, including a series based on a triazolo[4,5-d]pyrimidine scaffold, demonstrated cross-inhibition of PKR (***Lough et al., 2018***). Furthermore, the PKR inhibitor C16 has been shown to activate GCN2 in vitro (***Szaruga et al., 2023***). Intriguingly, viral infections or synthetic dsRNA known to activate PKR have also been shown to trigger GCN2 in some circumstances, though if this relates to structural similarities of their kinase domains has not been studied (***Szaruga et al., 2023***; ***Berlanga et al., 2006***; ***Krishnamoorthy et al., 2008***). While the functional relevance of PKR inhibition in our cellular systems is uncertain, these observations highlight the potential for kinase cross-reactivity, which will be important to address in future studies.

A remarkable finding in the current study was the lack of dependence on GCN1 for compound 20 to activate GCN2 in cells. During amino acid starvation, ribosome-associated GCN1 facilitates binding of uncharged tRNAs to GCN2, thus facilitating GCN2 activation (***Sattlegger and Hinnebusch, 2000***; ***Sattlegger and Hinnebusch, 2005***; ***Marton et al., 1993***). GCN1 also functions as a disome detector, enabling GCN2 activation in response to ribosome collisions (***Pochopien et al., 2021***). In genetic screens identifying modifiers of GCN2 activation by a small molecule, such as the dual HER2/EGFR inhibitor neratinib and the WEE1 inhibitor AZD1775, GCN1 has repeatedly been found to be necessary (***Tang et al., 2022***; ***Tjeerdsma et al., 2025***; ***Wilson et al., 2025***). We were able to confirm this GCN1 dependence for neratinib in the present study. It was therefore surprising that GCN2 activation by compound 20 did not appear to require GCN1 in human or hamster cells. While GCN1 is essential for the activation of GCN2 by amino acid starvation in yeast (***Hinnebusch, 1985***; ***Anda et al., 2017***), in vitro studies have shown that GCN2 activation by the ribosome P-stalk or by deacylated tRNAs does not absolutely require GCN1 (***Harding et al., 2019***; ***Inglis et al., 2019***). Yet we found compound 20 able to activate purified full-length human GCN2 to a far higher level than was possible with purified tRNAs. The markedly greater activation observed with compound 20 compared with uncharged tRNA in vitro raises the possibility that such compounds may partially bypass regulatory constraints on GCN2 activation, including those normally mediated by GCN1. Our modelling suggests that unlike neratinib, compound 20 can fit within the ATP pocket without needing to protrude into the solvent, nor extending deeply into the hydrophobic region beyond the gatekeeper Met802 residue towards the αC-helix. Indeed, analogues extending in these directions were inactive, perhaps suggesting value to this molecule's small size. This may prove useful as a tool compound for studies in which GCN1 is unavailable or non-functional.

There are limitations to our study. So far, our experiments have been limited to cultured cells, purified proteins, and in silico modelling. We have yet to test our compounds in an animal model. Although our pipeline excluded molecules showing toxicity, it is likely that prolonged activation of the ISR will have toxic consequences via targets including CHOP and PPP1R15A (***Marciniak et al., 2004***). Our most promising molecule, compound 20, contains a 2-aminothiazole. Although known to be a versatile scaffold, appearing in several clinically useful drugs including anti-inflammatory, anti-microbial and anticancer agents, 2-aminothiazole is sometimes considered a toxicophore owing to toxic consequences following its metabolism, and as a pan-assay interference compound (PAINS), owing to frequent false positives in high-throughput drug screens (***Das et al., 2016***; ***Jakopin, 2020***; ***Devine et al., 2015***). Our use of orthogonal approaches to support its activity as a GCN2 activator mitigates against it being a non-specific hit. Nevertheless, if this compound were to be developed further, attempts to 'design out' this feature by, for example, replacing the sulphur for an oxygen (thiazole to oxazole switch) could be attempted. Indeed, computational modelling reveals an adjacent NH which should form a stronger H-bond to oxygen of an oxazole, which may result in an improved potency to GCN2. Another potential limitation of our study is the use of existing analogues in SAR studies, the so-called 'analogue by catalogue' approach. Although less systematic than chemically synthesising further series de novo, it was cost effective and generated useful information on the tolerability of modifications of our lead scaffolds. Finally, our compounds were identified in a screen of CHO cells and appear to be more effective in these cells than in HeLa and 293T models. The absence of detectable activity in HeLa cells does not appear to be a species effect, since some activity was observed in human 293T cells and when using recombinant human GCN2 protein. It is likely therefore to reflect cell-type effects, since cancer cell lines are known to demonstrate dramatic differences in drug efficiency, even when using different strains of the same cell line (***Ben-David et al., 2018***). Moreover, histidinol-induced ISR activation showed a clear hierarchy across cell lines, with CHO cells being the most responsive and HeLa cells the least. We also evaluated the reported GCN2 activator HC-7366 in our CHO ATF4::NanoLuc reporter system. In this context, HC-7366 showed limited activity relative to compound 20, despite its reported efficacy in other cellular systems and in vivo (data not shown). This highlights potential context dependence in small-molecule activation of GCN2 and limits direct cross-study comparison. This should be considered carefully when using these compounds as tools or for further drug development.

In summary, we performed a chemical screen for novel activators of GCN2. We identified three chemically distinct scaffolds, and demonstrated one to be independent of the GCN2 cofactor GCN1.

Methods

Screen molecules

The initial screen used compounds sourced from the BioAscent library and all molecules dissolved in DMSO. Some follow-on compounds for SAR were sourced from Enamine. Subsequently, compound 18 was purchased from TimTec, USA (compound ST51216373). Compound 20 was synthesised by ChemBridge, USA (compound 5935953). Compound 21 was ordered from Specs, Netherlands (compound AC-907/25005415).

Cell lines

CHO, HeLa, COS-7, and HEK293T cells were originally obtained from the laboratory of Professor David Ron (Cambridge Institute for Medical Research, University of Cambridge, UK). HCT116 cells were obtained from the laboratory of Professor Simon Cook (Babraham Institute, Cambridge, UK). Mesobank 12T primary mesothelioma cells were obtained from Mesobank UK. Cell-line identity was verified on receipt by source provenance and subsequently monitored by characteristic morphology and experimental behaviour consistent with the reported cell type. STR profiling was not performed. No evidence of cell-line misidentification was encountered during this study. All cell lines were routinely tested for mycoplasma contamination and were negative.

NanoGlo luciferase assay

pGL4.2 ATF4-Nluc and pGL4.2 ATF4-Nluc-PEST were described previously (***Emanuelli et al., 2024***). In 384-well white microplate, test compounds, 3 mM histidinol or vehicle control were plated as 5x

solution in a volume of 5 µl in 10% FBS-Nutrient Mixture F-12 Ham supplemented with 1x GlutaMAX. CHO wild-type and *Eif2ak4*$^{-/-}$ ATF4::NanoLuc reporter cells were subsequently seeded at a density of 1.5 × 10^3 cells per well in 20 µl. After 16 hr at 37°C, NanoGlo luciferase assay reagent was added to each well and mixed with orbital shaking for 1 min. After 10 min of incubation at room temperature, bioluminescence signal (360–545 nm) was acquired on a Tecan Spark plate reader. Cells carrying an ATF4::nanoLuc-PEST reporter were used for live-cell assay, allowing detection of time-sensitive ATF4 signals (***Emanuelli et al., 2024***). Cells (1.25 × 10^4 cells per well) were plated overnight on white, clear bottom 96-well plate. Next day, 1 µl 100x Nano-Glo Endurazine substrate was mixed with cell culture medium and added to cells and incubated for 2 hr to reach stabilisation. Compounds were added to the wells and luminescence signals were measured using a Tecan CM Spark plate reader at 37°C in a humidity cassette for 48 hr. Data analysed using GraphPad Prism 10.

Bioluminescence resonance energy transfer

NanoBRET assay was performed according to the user's manual. Briefly, 4 × 10^5 cells/ml (HEK293T or CHO) were transfected with 100 ng of GCN2 kinase domain::nanoLuc reporter and 900 ng of transfection carrier DNA mixed in 100 µl Opti-mem (no phenol red) using lipofectamine LTX, and plated in 384-well cell-culture white microplates (40 µl/well, 8 × 10^3 cells). Twenty-two hours after transfection, tracer was added to each well and mixed on an orbital shaker. Test compound (final concentration 10, 30, and 100 µM), DMSO control (final concentration 0.1, 0.3, and 1%), and positive control GCN2iB (final concentration 1 µM) were added to each well and mixed. After 2 hr of incubation, NanoBRET Nano-Glo substrate-extracellular NanoLuc Inhibitor reagent was added to each well before bioluminescence measurement using a Tecan CM Spark plate reader (multi-colour measurement mode: wavelength 1, wavelength 445–470 nm, 300 ms integration; wavelength 2, wavelength 610–635 nm, 300 ms integration). Data analysed using GraphPad Prism 10.

Cell viability assay

Compounds were plated into 384-well white microplates and mixed with 20 µl of culture medium containing 1.5 × 10^3 cells per well, incubated for 16 hr at 37°C. CellTiter-Glo Assay reagent was added to each well for bioluminescence measurement using a Tecan CM Spark plate reader. Data analysed using GraphPad Prism 10.

Flow cytometry

CHOP::GFP and XBP1::Turquoise dual-reporter cells were treated with each compound (7.5–20 µM) and histidinol (0.75 mM) 18–20 hr prior to cell harvesting (***Sekine et al., 2016***). ER stress was induced using 2 µg/ml of tunicamycin. At the time of experiment, cells were trypsinised and collected by centrifugation, resuspended in 4 mM EDTA PBS, filtered through a 50-µm filter, then analysed using a DB Fortessa flow cytometer. GFP was measured at 530 nm and turquoise was measured at 450 nm. Data analysed using FlowJo software.

Quantitative real-time PCR

RNA was reverse transcribed to produce complementary DNA using High-Capacity cDNA Reverse Transcription Kit (Thermo, 4368814) according to the manufacturer's instructions. To perform real-time PCR, the PowerUp SYBR Green Master Mix (Thermo A25742) and the CFX96 Bio-Rad real-time PCR machine (Bio-Rad, UK) were used. All samples were measured in duplicate and included water control. Fold changes in expression were calculated using the ΔΔCt method. Hamster qPCR primers include

CHOP (Fw: GGGAGCTGGAAGCCTGGTAT, Rv: GGGACCCCCATTTTCATCTG),

PPP1R15A (Fw: CCTGGTCTGCAAAGTGCTGAT, Rv: CCAGCTCAGTCACTCCCTCTTC),

and β-actin (Fw: ACTCCTACGTGGGTGACGAG, Rv: AGGTGTGGTGCCAGATCTTC). Data analysed using GraphPad Prism 10.

Immunoblotting

Cells were washed with PBS on ice and lysed in low-salt buffer as previously described (***Emanuelli et al., 2024***). Following SDS–PAGE (7% gel for GCN2 and 14% gel for eIF2αor alternatively, 5–12% gradient gel), proteins were transferred to nitrocellulose membranes then analysed by immunoblotting. Antibodies used: total GCN2 (Gift from Ron lab: NY168); total GCN2 (1:1000, Invitrogen

JA03-83); GCN2-phosphorT899 (1:1000, Abcam, ab75836; RRID:AB_1310260); β-actin (1:5000, Abcam, ab8226; RRID:AB_306371); eIF2α phos-S51 (1:1000, Abcam, ab32157); eIF2α phos-S51 (1:500, Cell Signalling Technology 9721); total eIF2α (1:1000, Invitrogen, AHO0802); total eIF2α (Gift from David Ron lab, CIMR); total eIF2α (1:1000, Santa Cruz Biotechnology sc-133132).

Recombinant GCN2 kinase domain synthesis and in vitro kinase assay

The human GCN2 kinase domain (residues 585–1005) was tagged on its N-terminus with GST by cloning into the vector pGV67 by Gibson assembly. Protein was synthesised in BL21(DE3) *E. coli* Rosetta cells and purified using glutathione agarose beads. GCN2 kinase domain (0.3 µg) was incubated with 100 µM ATP, 1 µM eIF2α-NTD and test compounds in reaction buffer (50 mM HEPES, pH 7.4, 100 mM potassium acetate, 5 mM magnesium acetate, 250 µg/ml BSA, 10 mM magnesium chloride, 5 mM DTT, 5 mM β-glycerophosphate). Reactions were incubated at 32°C for 10 min, then immediately quenched with SDS sample buffer pre-warmed to 95°C. Samples were then analysed by immunoblotting.

Recombinant full-length GCN2 synthesis and in vitro kinase assay

Expression and purification of recombinant human GCN2 was conducted as described previously (***Inglis et al., 2019***). Briefly, human GCN2 (uniprot ID: Q9P2K8) was cloned into a baculoviral vector with an N-terminal twin StrepII tag followed by a TEV protease site. GCN2 was then expressed in *Sf9* cells grown at 27°C for 55 hr. Protein was purified using sequential StrepTrap HP column (GE Healthcare Life Sciences 28-9075-47), HiTrap Q HP column (Cytiva 17115401), Hi Load 16/60 Superdex 200 column (Cytiva/GE Healthcare 28989335). Ten nanomolar GCN2 was incubated at 30°C for 20 min with 2 µM eIF2α and 100 µM ATP in increasing concentrations (0.00169–100 µM) of deacylated tRNA or compound 20. Samples were then quenched via the addition of SDS-PAGE loading buffer and heating to 95°C for 3 min, then analysed by SDS–PAGE and immunoblotting: total eIF2α (Santa Cruz Biotechnology sc-133132) 1:1000, phospho-eIF2S1 Ser51 (Cell Signalling Technology 9721) 1:500, total GCN2 (Invitrogen JA03-83) 1:1000, and pThr899 GCN2 (Abcam AB75836) 1:1000. Images were captured and quantified in Image Studio Ver 5.2. Data analysed using GraphPad Prism 10.

Expression and purification of eIF2α

Expression and purification of recombinant human eIF2α was conducted as described previously (***Inglis et al., 2019***). DNA encoding full-length human eIF2α (NCBI reference number: NP_004085.1) was inserted into the vector pOPTH with an N-terminal His6 tag followed by a TEV protease site. Protein was expressed in BL21 Star (DE3) cells, at 37°C for 3 hr then purified using a HisTrap HP Column (Cytiva 17524801) as described for GCN2.

LanthaScreen in vitro kinase activity assay

In 384-well plate format, 1 nM human GCN2 (Carna Bioscience, # 05-153) or 1 nM human PERK (Carna Bioscience, # 05-155) or 2 nM human HRI (Carna Bioscience, # 05-154) or 3 nM human PKR (Carna Bioscience, # 05-156) were incubated with 50 mM HEPES pH 7.0, $MgCl_2$ 10 mM, $MnCl_2$ 5 mM, tRNA 4 µM (only for GCN2 assays), ATP (10 µM for GCN2, 0.1 µM for PERK, 0.15 µM for HRI, and 0.1 µM for PKR), GFP-eIF2α 80 nM. Reaction time was 20–30 min at room temperature, followed by detection time 50–60 min. TR-FRET signal between terbium-labelled antibody and GFP-labelled p-eIF2α read with excitation 340 nm and emission of the donor (terbium labelled anti-p-eIF2α antibody: 495 nm) and the acceptor (GFP-labelled p-eIF2α: 520 nm) on the Tecan Spark plate reader. IC_{50} values were determined in GraphPad Prism 8.0, using a 4-parameter model: log(inhibitor) vs response – variable slope.

In silico modelling

Five reported crystal structures for human GCN2 were considered PDB 6N3N, 6N3O, 6N3L, 7QWK, and 7QQ6 (***Fujimoto et al., 2019***; ***Maia de Oliveira et al., 2020***). Of these, 6N3N and 6N3L share ~100% sequence homology. While 6N3N has unresolved amino acid residues, these are remote from the ATP-binding site and should not impact the binding of the ligands. A visual inspection of 6N3O, 6N3N, and 6N3L highlighted that the activation loop in 6N3L is cut short and does not extend beyond the αC-helix, affecting the orientation of the DFG loop and its residues (Asp866, Phe867, and Gly868).

As such, 6N3L was not considered for further analysis. PDB sequences 7QWK and 7QQ6 share ~75% sequence homology, with 7QWK containing unresolved residues remote from the ATP-binding site. As observed with PDB 6N3L, the activation loop containing the DFG residues is cut short in both cases and does not extend beyond the αC-helix. Inspection of the binding mode of crystallised ligands of 7QQ6 and 7QWK demonstrates that these bind in a Type I-binding pocket, compared to Type II binding as observed in 6N3O.

Prior to docking, the protein structure (PDB ID: 6N3N) was put through the Protein Preparation Protocol of Maestro. This protocol added hydrogens, removed co-crystallised water molecules, optimised the receptor's hydrogen bond network, enumerated bond orders, and performed a restrained minimisation to alleviate backbone clashes with the receptor backbone. The protein was prepared at pH 7.4 (***Sastry et al., 2013***). SiteMap module was used on the prepared protein, with all settings set to default (SiteMap, Schrödinger Release 2024-4, Schrödinger, LLC, New York, http://www.schrodinger.com/). Grid generation was performed using the Glide Docking Protocol in Maestro (Glide, Schrödinger Release 2024-4, Schrödinger, LLC, New York, http://www.schrodinger.com/). This was centred around Met802 and Lys619. High-throughput virtual screening setting was used for docking.

Materials availability statement

The vector hGCN2-KinaseDomain-pGV67 generated for this work is available from the Marciniak lab subject to standard University of Cambridge MTA.

Acknowledgements

SJM was supported by the MRC (G1002610, MR/V028669/1, and MR/R009120/1), EPSRC (EP/R03558X/1), Cambridge Biomedical Research Centre (BRC-1215-20014); British Lung Foundation, Asthma+Lung UK, Royal Papworth Hospital, Alpha1 Foundation. GE was supported by philanthropic funding from Rick Medlock and by awards from EPSRC (EP/R03558X/1), BHF (RE/18/1/34212), Evelyn Trust (Grant 22/03), and the Cambridge-Tsinghua collaborative programme on sustainability and emerging technologies. JZ was supported by the Doctoral Training Programme in Medical Research (DTP-MR; Cambridge Trust). GRM is supported by a Baxter Fellowship from the University of Dundee, and a TENOVUS grant T21/01 119615, and Biotechnology and Biological Sciences Research Council (UKRI-BBSRC) Capital Equipment Grant BB/V019635/1. VV supported by MRC iCase Studentship (MR/R01579/1). This research was supported by the CIMR Flow Cytometry Core Facility. We wish to thank Reiner Schulte and Gabriela Grondys-Kotarba for their advice and support in flow cytometry cell sorting. We wish to thank Heather Harding for helpful discussions and reagents. We wish to thank Steve Andrews, Kushal Rugjee, and other colleagues at the ADDI for help with chemical library preparation. Thanks to Apollo Therapeutics Ltd for conducting the LanthaScreen in vitro kinase activity at Selvita S.A, Krakow, Poland.

Additional information

Competing interests

Fergus Preston: employee of Domainex Ltd. The other authors declare that no competing interests exist.

Funding

Funder	Grant reference number	Author
Cambridge Trust		JiaYi Zhu
University of Cambridge		JiaYi Zhu
Medical Research Council	G1002610	Stefan J Marciniak
Medical Research Council	MR/V028669/1	Stefan J Marciniak
Medical Research Council	MR/R009120/1	Stefan J Marciniak

Funder	Grant reference number	Author
Engineering and Physical Sciences Research Council	EP/R03558X/1	Stefan J Marciniak Giulia Emanuelli
Cambridge Biomedical Research Centre	BRC-1215-20014	Stefan J Marciniak
British Heart Foundation	RE/18/1/34212	Giulia Emanuelli Stefan J Marciniak Nicholas W Morrell
Evelyn Trust	22/03	Giulia Emanuelli
Tenovus Scotland	T21/01 119615	Glenn Robert Masson
Biotechnology and Biological Sciences Research Council	BB/V019635/1	Glenn Robert Masson
Medical Research Council	MR/R01579/1	Vanessa Vinciauskaite
Asthma + Lung UK		Stefan J Marciniak
Royal Papworth Hospital		Stefan J Marciniak
Alpha1 Foundation		Stefan J Marciniak
University of Dundee	Baxter Fellowship	Glenn Robert Masson

The funders had no role in study design, data collection, and interpretation, or the decision to submit the work for publication.

Author contributions

JiaYi Zhu, Conceptualization, Data curation, Formal analysis, Validation, Investigation, Visualization, Methodology, Writing – original draft, Writing – review and editing; Giulia Emanuelli, Conceptualization, Software, Formal analysis, Validation, Investigation, Visualization, Methodology, Writing – original draft, Writing – review and editing; Glenn Robert Masson, Rebecca Gilley, John Skidmore, Resources, Investigation, Methodology, Writing – original draft, Writing – review and editing; Vanessa Vinciauskaite, Peiqiao Cai, Investigation; Henriette Willems, Andrew Lim, Christopher Alan Brown, David Winpenny, Investigation, Methodology; Murray Clarke, Investigation, Methodology, Writing – original draft, Writing – review and editing; Fergus Preston, Software, Investigation, Visualization, Methodology, Writing – original draft, Writing – review and editing; Jordan CJ Wilson, Aldo Bader, Resources, Investigation, Methodology; Taufiq Rahman, Resources, Software, Supervision, Investigation, Writing – original draft, Writing – review and editing; Joseph E Chambers, Conceptualization, Supervision, Methodology, Writing – original draft, Writing – review and editing; Nicholas W Morrell, Conceptualization, Supervision, Funding acquisition, Investigation, Methodology, Writing – original draft, Writing – review and editing; Stefan J Marciniak, Conceptualization, Resources, Formal analysis, Supervision, Funding acquisition, Validation, Investigation, Visualization, Methodology, Writing – original draft, Project administration, Writing – review and editing

Author ORCIDs

JiaYi Zhu https://orcid.org/0000-0001-7401-6468
Giulia Emanuelli https://orcid.org/0000-0001-8899-6110
Glenn Robert Masson https://orcid.org/0000-0002-1386-4719
Henriette Willems https://orcid.org/0000-0001-7196-5975
Joseph E Chambers https://orcid.org/0000-0003-4675-0053
Stefan J Marciniak https://orcid.org/0000-0001-8472-7183

Peer review material

Version of Record:

Reviewer #1 (Public review): https://doi.org/10.7554/eLife.108590.3.sa1
Reviewer #2 (Public review): https://doi.org/10.7554/eLife.108590.3.sa2
Reviewer #3 (Public review): https://doi.org/10.7554/eLife.108590.3.sa3
Author response https://doi.org/10.7554/eLife.108590.3.sa4

Reviewed preprint v2
Reviewer #1 (Public review): https://doi.org/10.7554/eLife.108590.2.sa3
Reviewer #2 (Public review): https://doi.org/10.7554/eLife.108590.2.sa2
Reviewer #3 (Public review): https://doi.org/10.7554/eLife.108590.2.sa1
Author response: https://doi.org/10.7554/eLife.108590.2.sa0
eLife Assessment https://doi.org/10.7554/eLife.108590.2.sa4

Reviewed preprint v1
Reviewer #1 (Public review): https://doi.org/10.7554/eLife.108590.1.sa3
Reviewer #2 (Public review): https://doi.org/10.7554/eLife.108590.1.sa2
Reviewer #3 (Public review): https://doi.org/10.7554/eLife.108590.1.sa1
Author response: https://doi.org/10.7554/eLife.108590.1.sa0
eLife Assessment https://doi.org/10.7554/eLife.108590.1.sa4

Additional files

Supplementary files

MDAR checklist

Data availability

Uncropped blots have been uploaded as ***Figure 2—source data 1*** and ***Figure 5—source data 1***. Raw image files have been uploaded as ***Figure 2—source data 2*** and ***Figure 5—source data 2***.

References

Anda S, Zach R, Grallert B. 2017. Activation of Gcn2 in response to different stresses. *PLOS ONE* **12**:e0182143. DOI: https://doi.org/10.1371/journal.pone.0182143, PMID: 28771613

Ben-David U, Siranosian B, Ha G, Tang H, Oren Y, Hinohara K, Strathdee CA, Dempster J, Lyons NJ, Burns R, Nag A, Kugener G, Cimini B, Tsvetkov P, Maruvka YE, O'Rourke R, Garrity A, Tubelli AA, Bandopadhayay P, Tsherniak A, et al. 2018. Genetic and transcriptional evolution alters cancer cell line drug response. *Nature* **560**:325–330. DOI: https://doi.org/10.1038/s41586-018-0409-3, PMID: 30089904

Berlanga JJ, Ventoso I, Harding HP, Deng J, Ron D, Sonenberg N, Carrasco L, de Haro C. 2006. Antiviral effect of the mammalian translation initiation factor 2alpha kinase GCN2 against RNA viruses. *The EMBO Journal* **25**:1730–1740. DOI: https://doi.org/10.1038/sj.emboj.7601073, PMID: 16601681

Bou-Nader C, Gaikwad S, Bahmanjah S, Zhang F, Hinnebusch AG, Zhang J. 2024. Gcn2 structurally mimics and functionally repurposes the HisRS enzyme for the integrated stress response. *PNAS* **121**:e2409628121. DOI: https://doi.org/10.1073/pnas.2409628121, PMID: 39163341

Carlson KR, Georgiadis MM, Tameire F, Staschke KA, Wek RC. 2023. Activation of Gcn2 by small molecules designed to be inhibitors. *The Journal of Biological Chemistry* **299**:104595. DOI: https://doi.org/10.1016/j.jbc.2023.104595, PMID: 36898579

Chakrabarty Y, Yang Z, Chen H, Chan DC. 2024. The HRI branch of the integrated stress response selectively triggers mitophagy. *Molecular Cell* **84**:1090–1100. DOI: https://doi.org/10.1016/j.molcel.2024.01.016, PMID: 38340717

Chambers JE, Dalton LE, Clarke HJ, Malzer E, Dominicus CS, Patel V, Moorhead G, Ron D, Marciniak SJ. 2015. Actin dynamics tune the integrated stress response by regulating eukaryotic initiation factor 2α dephosphorylation. *eLife* **4**:e04872. DOI: https://doi.org/10.7554/eLife.04872, PMID: 25774599

Dalton LE, Healey E, Irving J, Marciniak SJ. 2012. Phosphoproteins in stress-induced disease. *Progress in Molecular Biology and Translational Science* **106**:189–221. DOI: https://doi.org/10.1016/B978-0-12-396456-4.00003-1, PMID: 22340719

Das D, Sikdar P, Bairagi M. 2016. Recent developments of 2-aminothiazoles in medicinal chemistry. *European Journal of Medicinal Chemistry* **109**:89–98. DOI: https://doi.org/10.1016/j.ejmech.2015.12.022, PMID: 26771245

Devine SM, Mulcair MD, Debono CO, Leung EWW, Nissink JWM, Lim SS, Chandrashekaran IR, Vazirani M, Mohanty B, Simpson JS, Baell JB, Scammells PJ, Norton RS, Scanlon MJ. 2015. Promiscuous 2-aminothiazoles (PrATs): a frequent hitting scaffold. *Journal of Medicinal Chemistry* **58**:1205–1214. DOI: https://doi.org/10.1021/jm501402x, PMID: 25559643

Dong J, Qiu H, Garcia-Barrio M, Anderson J, Hinnebusch AG. 2000. Uncharged tRNA activates GCN2 by displacing the protein kinase moiety from a bipartite tRNA-binding domain. *Molecular Cell* **6**:269–279. DOI: https://doi.org/10.1016/s1097-2765(00)00028-9, PMID: 10983975

Drainas AP, Hsu W-H, Dallas AE, Poltorack CD, Kim JW, He A, Coles GL, Baron M, Bassik MC, Sage J. 2024. GCN2 is a determinant of the response to WEE1 kinase inhibition in small-cell lung cancer. *Cell Reports* **43**:114606. DOI: https://doi.org/10.1016/j.celrep.2024.114606, PMID: 39120974

Emanuelli G, Nassehzadeh-Tabriz N, Morrell NW, Marciniak SJ. 2020. The integrated stress response in pulmonary disease. *European Respiratory Review* **29**:200184. DOI: https://doi.org/10.1183/16000617.0184-2020, PMID: 33004527

Emanuelli G, Zhu J, Li W, Morrell NW, Marciniak SJ. 2024. Functional validation of EIF2AK4 (GCN2) missense variants associated with pulmonary arterial hypertension. *Human Molecular Genetics* **33**:1495–1505. DOI: https://doi.org/10.1093/hmg/ddae082, PMID: 38776952

Fujimoto J, Kurasawa O, Takagi T, Liu X, Banno H, Kojima T, Asano Y, Nakamura A, Nambu T, Hata A, Ishii T, Sameshima T, Debori Y, Miyamoto M, Klein MG, Tjhen R, Sang BC, Levin I, Lane SW, Snell GP, et al. 2019. Identification of novel, potent, and orally available GCN2 inhibitors with type I half binding mode. *ACS Medicinal Chemistry Letters* **10**:1498–1503. DOI: https://doi.org/10.1021/acsmedchemlett.9b00400, PMID: 31620240

Garcia-Barrio M, Dong J, Ufano S, Hinnebusch AG. 2000. Association of GCN1-GCN20 regulatory complex with the N-terminus of eIF2alpha kinase GCN2 is required for GCN2 activation. *The EMBO Journal* **19**:1887–1899. DOI: https://doi.org/10.1093/emboj/19.8.1887, PMID: 10775272

Gilley R, Kidger AM, Neill G, Severson P, Byrne DP, Kenneth NS, Bollag G, Zhang C, de Oliveira TM, Eyers PA, Bayliss R, Masson GR, Cook SJ. 2024. RAF inhibitors activate the integrated stress response by direct activation of GCN2. *bioRxiv*. DOI: https://doi.org/10.1101/2024.08.15.607884

Grummt F, Grummt I. 1976. Studies on the role of uncharged tRNA in pleiotypic response of animal cells. *European Journal of Biochemistry* **64**:307–312. DOI: https://doi.org/10.1111/j.1432-1033.1976.tb10302.x, PMID: 1278158

Guo L, Shao W, Zhou C, Yang H, Yang L, Cai Q, Wang J, Shi Y, Huang L, Zhang J. 2023. Neratinib for HER2-positive breast cancer with an overlooked option. *Molecular Medicine* **29**:134. DOI: https://doi.org/10.1186/s10020-023-00736-0, PMID: 37803271

Gupta R, Hinnebusch AG. 2023. Differential requirements for P stalk components in activating yeast protein kinase Gcn2 by stalled ribosomes during stress. *PNAS* **120**:e2300521120. DOI: https://doi.org/10.1073/pnas.2300521120

Hansen BS, Vaughan MH, Wang L. 1972. Reversible inhibition by histidinol of protein synthesis in human cells at the activation of histidine. *The Journal of Biological Chemistry* **247**:3854–3857 PMID: 4338230.

Harding HP, Zhang Y, Ron D. 1999. Protein translation and folding are coupled by an endoplasmic-reticulum-resident kinase. *Nature* **397**:271–274. DOI: https://doi.org/10.1038/16729, PMID: 9930704

Harding HP, Zhang Y, Zeng H, Novoa I, Lu PD, Calfon M, Sadri N, Yun C, Popko B, Paules R, Stojdl DF, Bell JC, Hettmann T, Leiden JM, Ron D. 2003. An integrated stress response regulates amino acid metabolism and resistance to oxidative stress. *Molecular Cell* **11**:619–633. DOI: https://doi.org/10.1016/s1097-2765(03)00105-9, PMID: 12667446

Harding HP, Ordonez A, Allen F, Parts L, Inglis AJ, Williams RL, Ron D. 2019. The ribosomal P-stalk couples amino acid starvation to GCN2 activation in mammalian cells. *eLife* **8**:e50149. DOI: https://doi.org/10.7554/eLife.50149, PMID: 31749445

Hinnebusch AG. 1985. A hierarchy of trans-acting factors modulates translation of an activator of amino acid biosynthetic genes in *Saccharomyces cerevisiae*. *Molecular and Cellular Biology* **5**:2349–2360. DOI: https://doi.org/10.1128/mcb.5.9.2349-2360.1985, PMID: 3915540

Hinnebusch AG, Lorsch JR. 2012. The mechanism of eukaryotic translation initiation: new insights and challenges. *Cold Spring Harbor Perspectives in Biology* **4**:a011544. DOI: https://doi.org/10.1101/cshperspect.a011544, PMID: 22815232

Ill CR, Marikar NC, Nguyen V, Nangia V, Darnell AM, Vander Heiden MG, Reigan P, Spencer SL. 2024. $BRAF^{V600}$ and ErbB inhibitors directly activate GCN2 in an off-target manner to limit cancer cell proliferation. *bioRxiv*. DOI: https://doi.org/10.1101/2024.12.19.629301

Inglis AJ, Masson GR, Shao S, Perisic O, McLaughlin SH, Hegde RS, Williams RL. 2019. Activation of GCN2 by the ribosomal P-stalk. *PNAS* **116**:4946–4954. DOI: https://doi.org/10.1073/pnas.1813352116, PMID: 30804176

Jadhav M, Sankhe K, Bhandare RR, Edis Z, Bloukh SH, Khan TA. 2021. Synthetic strategies of pyrimidine-based scaffolds as aurora kinase and polo-like kinase inhibitors. *Molecules* **26**:5170. DOI: https://doi.org/10.3390/molecules26175170, PMID: 34500603

Jakopin Ž. 2020. 2-aminothiazoles in drug discovery: privileged structures or toxicophores? *Chemico-Biological Interactions* **330**:109244. DOI: https://doi.org/10.1016/j.cbi.2020.109244, PMID: 32861748

Krishnamoorthy J, Mounir Z, Raven JF, Koromilas AE. 2008. The eIF2alpha kinases inhibit vesicular stomatitis virus replication independently of eIF2alpha phosphorylation. *Cell Cycle* **7**:2346–2351. DOI: https://doi.org/10.4161/cc.6323, PMID: 18677106

Kubota H, Sakaki Y, Ito T. 2000. GI domain-mediated association of the eukaryotic initiation factor 2alpha kinase GCN2 with its activator GCN1 is required for general amino acid control in budding yeast. *The Journal of Biological Chemistry* **275**:20243–20246. DOI: https://doi.org/10.1074/jbc.C000262200, PMID: 10801780

Lough L, Sherman D, Beccera-Flores M, Lavinda O, Ni E, Wang H, Tibes R, Cardozo T. 2018. Triazolo[4,5-*d*] pyrimidines as validated General Control Nonderepressible 2 (GCN2) protein kinase inhibitors reduce growth of leukemia cells. *Computational and Structural Biotechnology Journal* **16**:350–360. DOI: https://doi.org/10.1016/j.csbj.2018.09.003, PMID: 30364637

Lu PD, Harding HP, Ron D. 2004. Translation reinitiation at alternative open reading frames regulates gene expression in an integrated stress response. *The Journal of Cell Biology* **167**:27–33. DOI: https://doi.org/10.1083/jcb.200408003, PMID: 15479734

Maia de Oliveira T, Korboukh V, Caswell S, Winter Holt JJ, Lamb M, Hird AW, Overman R. 2020. The structure of human GCN2 reveals a parallel, back-to-back kinase dimer with a plastic DFG activation loop motif. *The Biochemical Journal* **477**:275–284. DOI: https://doi.org/10.1042/BCJ20190196, PMID: 31868900

Marciniak SJ, Yun CY, Oyadomari S, Novoa I, Zhang Y, Jungreis R, Nagata K, Harding HP, Ron D. 2004. CHOP induces death by promoting protein synthesis and oxidation in the stressed endoplasmic reticulum. *Genes & Development* **18**:3066–3077. DOI: https://doi.org/10.1101/gad.1250704

Marciniak SJ, Garcia-Bonilla L, Hu J, Harding HP, Ron D. 2006. Activation-dependent substrate recruitment by the eukaryotic translation initiation factor 2 kinase PERK. *The Journal of Cell Biology* **172**:201–209. DOI: https://doi.org/10.1083/jcb.200508099, PMID: 16418533

Marciniak SJ, Chambers JE, Ron D. 2022. Pharmacological targeting of endoplasmic reticulum stress in disease. *Nature Reviews. Drug Discovery* **21**:115–140. DOI: https://doi.org/10.1038/s41573-021-00320-3, PMID: 34702991

Marton MJ, Crouch D, Hinnebusch AG. 1993. GCN1, a translational activator of GCN4 in *Saccharomyces cerevisiae*, is required for phosphorylation of eukaryotic translation initiation factor 2 by protein kinase GCN2. *Molecular and Cellular Biology* **13**:3541–3556. DOI: https://doi.org/10.1128/mcb.13.6.3541-3556.1993, PMID: 8497269

Masson GR. 2019. Towards a model of GCN2 activation. *Biochemical Society Transactions* **47**:1481–1488. DOI: https://doi.org/10.1042/BST20190331, PMID: 31647517

Matts RL, Levin DH, London IM. 1983. Effect of phosphorylation of the alpha-subunit of eukaryotic initiation factor 2 on the function of reversing factor in the initiation of protein synthesis. *PNAS* **80**:2559–2563. DOI: https://doi.org/10.1073/pnas.80.9.2559, PMID: 6573671

Neill G, Vinciauskaite V, Paul M, Gilley R, Cook SJ, Masson GR. 2024. Paradoxical activation of GCN2 by ATP-competitive inhibitors via allosteric activation and autophosphorylation. *bioRxiv*. DOI: https://doi.org/10.1101/2024.08.14.606984

Novoa I, Zeng H, Harding HP, Ron D. 2001. Feedback inhibition of the unfolded protein response by GADD34-mediated dephosphorylation of eIF2alpha. *The Journal of Cell Biology* **153**:1011–1022. DOI: https://doi.org/10.1083/jcb.153.5.1011, PMID: 11381086

Oliveira MM, Mohamed M, Elder MK, Banegas-Morales K, Mamcarz M, Lu EH, Golhan EAN, Navrange N, Chatterjee S, Abel T, Klann E. 2024. The integrated stress response effector GADD34 is repurposed by neurons to promote stimulus-induced translation. *Cell Reports* **43**:113670. DOI: https://doi.org/10.1016/j.celrep.2023.113670, PMID: 38219147

Pacey S, Leung C, Rodney S, DosReis AFP, Ruddle R, Tall M, Swales K, Poele RT, Workman P, Marsolini D, Sardone M, Poradosu E, Shemesh S, Banerji U. 2024. Abstract CT111: pharmacokinetic and pharmacodynamic evaluation of NXP800, a novel GCN2 activator, in a first in human clinical trial. *Cancer Research* **84**:CT111. DOI: https://doi.org/10.1158/1538-7445.AM2024-CT111

Pochopien AA, Beckert B, Kasvandik S, Berninghausen O, Beckmann R, Tenson T, Wilson DN. 2021. Structure of Gcn1 bound to stalled and colliding 80S ribosomes. *PNAS* **118**:e2022756118. DOI: https://doi.org/10.1073/pnas.2022756118, PMID: 33790014

Robers MB, Wilkinson JM, Vasta JD, Berger LM, Berger BT, Knapp S. 2021. Single tracer-based protocol for broad-spectrum kinase profiling in live cells with NanoBRET. *STAR Protocols* **2**:100822. DOI: https://doi.org/10.1016/j.xpro.2021.100822, PMID: 34568844

Roskoski R Jr. 2016. Classification of small molecule protein kinase inhibitors based upon the structures of their drug-enzyme complexes. *Pharmacological Research* **103**:26–48. DOI: https://doi.org/10.1016/j.phrs.2015.10.021, PMID: 26529477

Sastry GM, Adzhigirey M, Day T, Annabhimoju R, Sherman W. 2013. Protein and ligand preparation: parameters, protocols, and influence on virtual screening enrichments. *Journal of Computer-Aided Molecular Design* **27**:221–234. DOI: https://doi.org/10.1007/s10822-013-9644-8, PMID: 23579614

Sattlegger E, Hinnebusch AG. 2000. Separate domains in GCN1 for binding protein kinase GCN2 and ribosomes are required for GCN2 activation in amino acid-starved cells. *The EMBO Journal* **19**:6622–6633. DOI: https://doi.org/10.1093/emboj/19.23.6622, PMID: 11101534

Sattlegger E, Hinnebusch AG. 2005. Polyribosome binding by GCN1 is required for full activation of eukaryotic translation initiation factor 2{alpha} kinase GCN2 during amino acid starvation. *The Journal of Biological Chemistry* **280**:16514–16521. DOI: https://doi.org/10.1074/jbc.M414566200, PMID: 15722345

Sekine Y, Zyryanova A, Crespillo-Casado A, Amin-Wetzel N, Harding HP, Ron D. 2016. Paradoxical sensitivity to an integrated stress response blocking mutation in vanishing white matter cells. *PLOS ONE* **11**:e0166278. DOI: https://doi.org/10.1371/journal.pone.0166278, PMID: 27812215

Snieckute G, Genzor AV, Vind AC, Ryder L, Stoneley M, Chamois S, Dreos R, Nordgaard C, Sass F, Blasius M, López AR, Brynjólfsdóttir SH, Andersen KL, Willis AE, Frankel LB, Poulsen SS, Gatfield D, Gerhart-Hines Z, Clemmensen C, Bekker-Jensen S. 2022. Ribosome stalling is a signal for metabolic regulation by the ribotoxic stress response. *Cell Metabolism* **34**:2036–2046.. DOI: https://doi.org/10.1016/j.cmet.2022.10.011, PMID: 36384144

Solorio-Kirpichyan K, Fan X, Golovenko D, Korostelev AA, Yan N, Korennykh A. 2024. Cryo-EM structure of histidyl-tRNA synthetase-like domain reveals activating crossed helices at the core of GCN2. *PNAS Nexus* **3**:pgae528. DOI: https://doi.org/10.1093/pnasnexus/pgae528, PMID: 39618511

Szaruga M, Janssen DA, de Miguel C, Hodgson G, Fatalska A, Pitera AP, Andreeva A, Bertolotti A. 2023. Activation of the integrated stress response by inhibitors of its kinases. *Nature Communications* **14**:5535. DOI: https://doi.org/10.1038/s41467-023-40823-8, PMID: 37684277

Tang CP, Clark O, Ferrarone JR, Campos C, Lalani AS, Chodera JD, Intlekofer AM, Elemento O, Mellinghoff IK. 2022. GCN2 kinase activation by ATP-competitive kinase inhibitors. *Nature Chemical Biology* **18**:207–215. DOI: https://doi.org/10.1038/s41589-021-00947-8

Tjeerdsma RB, Ng TF, Roorda M, Bianchi D, Yang S, Bonnet C, VanInsberghe M, Everts M, Bakker FJ, de Boer HR, Moatti N, Hustedt N, Yin J, Hoeg L, Leibovitch M, Sicheri F, van Oudenaarden A, de Jong S, van den Berg J, Tanenbaum ME, et al. 2025. WEE1 inhibitors trigger GCN2-mediated activation of the integrated stress response. *bioRxiv*. DOI: https://doi.org/10.1101/2025.03.12.642754

Wek SA, Zhu S, Wek RC. 1995. The histidyl-tRNA synthetase-related sequence in the eIF-2 alpha protein kinase GCN2 interacts with tRNA and is required for activation in response to starvation for different amino acids. *Molecular and Cellular Biology* **15**:4497–4506. DOI: https://doi.org/10.1128/MCB.15.8.4497, PMID: 7623840

Wilson JCJ, Zhu J, Lam S, Hart A, Goh CG, Bou-Dagher F, Razumkov H, Kobel L, Kontarakis Z, Fielden J, Schlapansky MF, Loizou JI, Villunger A, Corn JE, Marciniak SJ, Bader AS, Jackson SP. 2025. WEE1 inhibitors synergise with mrna translation defects via activation of the kinase GCN2. *bioRxiv*. DOI: https://doi.org/10.1101/2025.03.12.642825

Wu CCC, Peterson A, Zinshteyn B, Regot S, Green R. 2020. Ribosome collisions trigger general stress responses to regulate cell fate. *Cell* **182**:404–416. DOI: https://doi.org/10.1016/j.cell.2020.06.006, PMID: 32610081

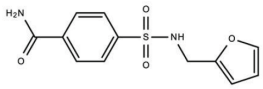
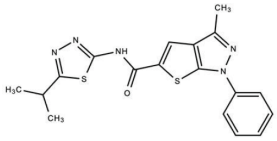
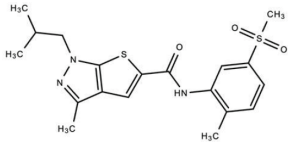
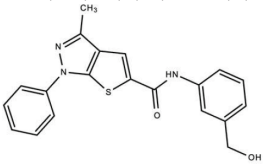
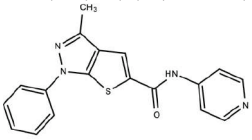
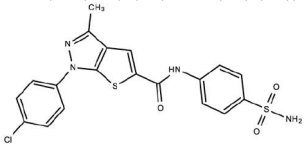
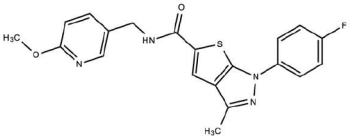
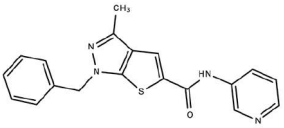
Wu Y, Yang Y, Qin X, Zhang Z, Ullah M, Li Y, Zhang Z. 2024. Unfolded proteins in the mitochondria activate HRI and inhibit mitochondrial protein translation. *Cellular Signalling* **123**:111353. DOI: https://doi.org/10.1016/j.cellsig.2024.111353

Yin JZ, Keszei AFA, Houliston S, Filandr F, Beenstock J, Daou S, Kitaygorodsky J, Schriemer DC, Mazhab-Jafari MT, Gingras AC, Sicheri F. 2024. The HisRS-like domain of GCN2 is a pseudoenzyme that can bind uncharged tRNA. *Structure* **32**:795–811. DOI: https://doi.org/10.1016/j.str.2024.02.021, PMID: 38531363

Zhu S, Nguyen A, Pang J, Zhao J, Chen Z, Liang Z, Gu Y, Huynh H, Bao Y, Lee S, Kluger Y, Ouyang K, Evans SM, Fang X. 2022. Mitochondrial stress induces an HRI-eIF2α pathway protective for cardiomyopathy. *Circulation* **146**:1028–1031. DOI: https://doi.org/10.1161/CIRCULATIONAHA.122.059594, PMID: 36154620

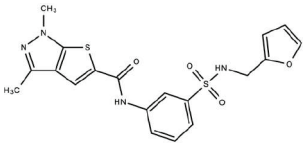
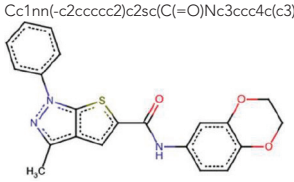
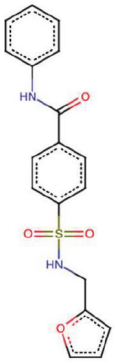
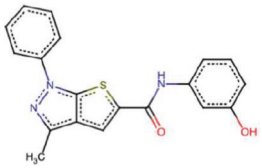
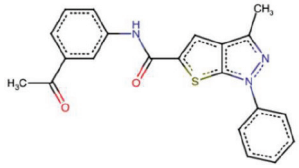
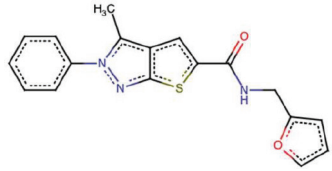
Appendix 1

Appendix 1—table 1. Structure-activity analysis of compound 20 and related analogues.

Structure of compound 18 analogue and fragment	ID	ISR activation	GCN2 specificity
NC(=O)c1ccc(cc1)S(=O)(=O)NCc1ccco1 	Z33546257	-	NA
CC(C)c1nnc(s1)NC(=O)c1cc2c(nn(c2s1)-c1ccccc1)C 	Z56783036	-	NA
CC(C)Cn1nc(c2cc(sc12)C(=O)Nc1cc(ccc1C)S(=O)(=O)C)C 	Z88478561	-	NA
Cc1nn(c2sc(cc12)C(=O)Nc1cccc(c1)CO)-c1ccccc1 	Z28913272	+	NA
Cc1nn(c2sc(cc12)C(=O)Nc1ccncc1)-c1ccccc1 	Z85517350	++	NA
Cc1nn(c2sc(cc12)C(=O)Nc1ccc(cc1)S(=O)(=O)N)-c1ccc(cc1)Cl 	Z27682945	+	NA
COc1ccc(cn1)CNC(=O)c1cc2c(nn(c2s1)-c1ccc(cc1)F)C 	Z226209130	-	NA
Cc1nn(c2sc(cc12)C(=O)Nc1cccnc1)Cc1ccccc1 	Z117416778	+	NA

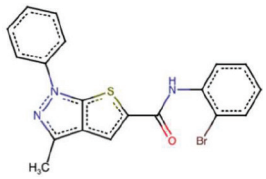
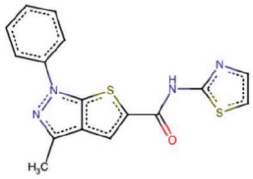
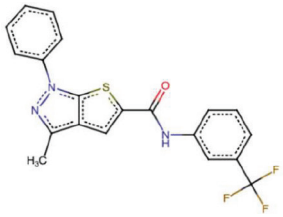
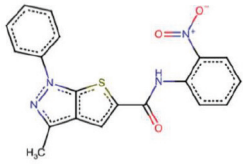
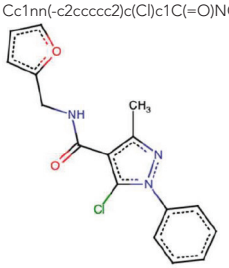
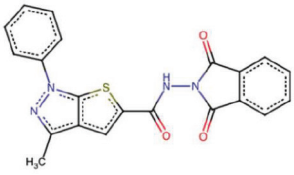
Appendix 1—table 1 Continued on next page

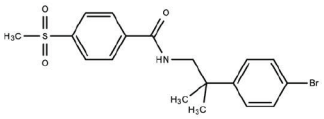
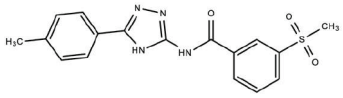
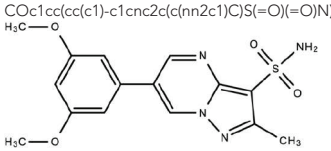
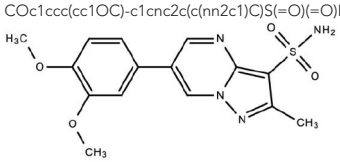
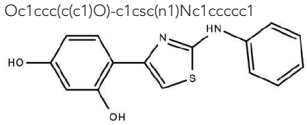
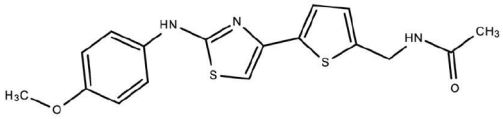
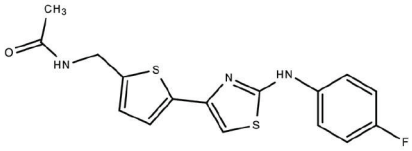
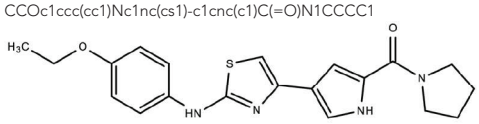
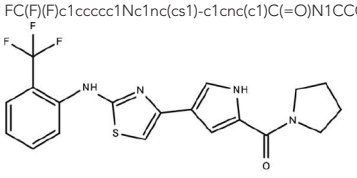
Appendix 1—table 1 Continued

Structure of compound 18 analogue and fragment	ID	ISR activation	GCN2 specificity
Cc1nn(c2sc(cc12)C(=O)Nc1cccc(c1)S(=O)(=O)NCc1ccco1)C 	Z228719934	-	NA
Cc1nn(-c2ccccc2)c2sc(C(=O)Nc3ccc4c(c3)OCCO4)cc12 	BCC0077119	+	+
O=C(Nc1ccccc1)c1ccc(S(=O)(=O)NCc2ccco2)cc1 	BCC0112913	-	NA
Cc1nn(-c2ccccc2)c2sc(C(=O)Nc3cccc(O)c3)cc12 	BCC0106222	++	-
CC(=O)c1cccc(NC(=O)c2cc3c(C)nn(-c4ccccc4)c3s2)c1 	BCC0104214	+	NA
Cc1c2cc(C(=O)NCc3ccco3)sc2nn1-c1ccccc1 	BCC0040387	-	NA

Appendix 1—table 1 Continued on next page

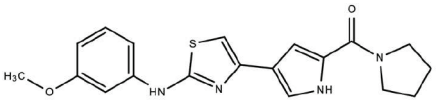
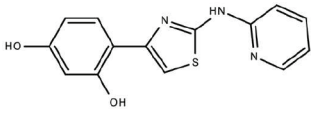
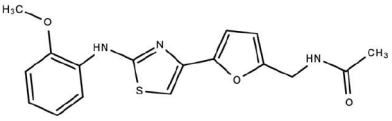
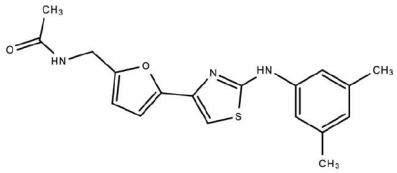
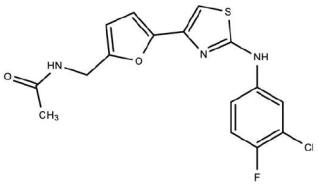
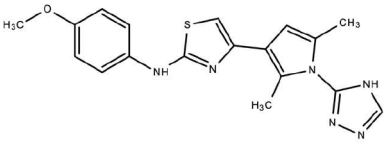
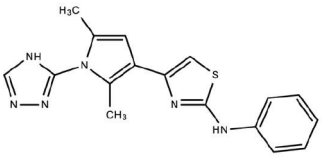
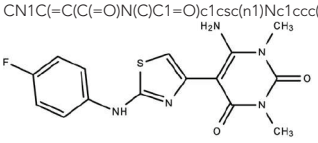
Appendix 1—table 1 Continued

Structure of compound 18 analogue and fragment	ID	ISR activation	GCN2 specificity
Cc1nn(-c2ccccc2)c2sc(C(=O)Nc3ccccc3Br)cc12 	BCC0113320	+	+
Cc1nn(-c2ccccc2)c2sc(C(=O)Nc3nccs3)cc12 	BCC0073142	-	NA
Cc1nn(-c2ccccc2)c2sc(C(=O)Nc3cccc(C(F)(F)F)c3)cc12 	BCC0043997	-	NA
Cc1nn(-c2ccccc2)c2sc(C(=O)Nc3ccccc3[N+](=O)[O-])cc12 	BCC0073242	-	NA
Cc1nn(-c2ccccc2)c(Cl)c1C(=O)NCc1ccco1 	BCC0104192	-	NA
Cc1nn(-c2ccccc2)c2sc(C(=O)NN3C(=O)c4ccccc4C3=O)cc12 	BCC0074259	-	NA

Structure of compound 21 analogue and fragment	ID	ISR activation	GCN2 specificity
CC(C)(CNC(=O)c1ccc(cc1)S(=O)(=O)C)c1ccc(cc1)Br 	Z423087112	-	NA
Cc1ccc(cc1)-c1nnc([nH]1)NC(=O)c1cccc(c1)S(=O)(=O)C 	Z119766318	-	NA
COc1cc(cc(c1)-c1cnc2c(c(nn2c1)C)S(=O)(=O)N)OC 	Z3464816516	-	NA
COc1ccc(cc1OC)-c1cnc2c(c(nn2c1)C)S(=O)(=O)N 	Z3464816527	-	NA
Structure of compound 20 analogue and fragment	**ID**	**ISR activation**	**GCN2 specificity**
Oc1ccc(c(c1)O)-c1csc(n1)Nc1ccccc1 	Z48853885	-	NA
COc1ccc(cc1)Nc1nc(cs1)-c1ccc(s1)CNC(=O)C 	Z73485298	-	NA
CC(=O)NCc1ccc(s1)-c1csc(n1)Nc1ccc(cc1)F 	Z118606822	-	NA
CCOc1ccc(cc1)Nc1nc(cs1)-c1cnc(c1)C(=O)N1CCCC1 	Z134826202	++	NA
FC(F)(F)c1ccccc1Nc1nc(cs1)-c1cnc(c1)C(=O)N1CCCC1 	Z134826094	+	NA

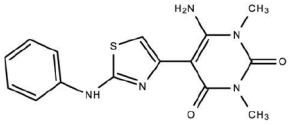
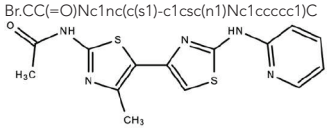
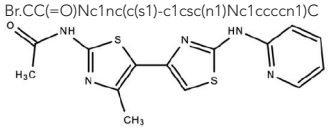
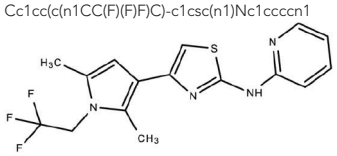
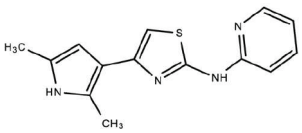
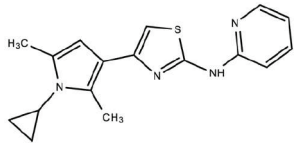
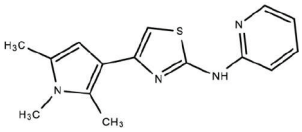
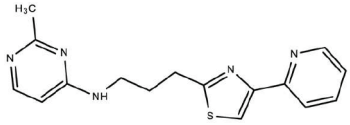
Continued on next page

Continued

Structure of compound 20 analogue and fragment	ID	ISR activation	GCN2 specificity
COc1cccc(c1)Nc1nc(cs1)-c1cnc(c1)C(=O)N1CCCC1 	Z134826982	++	NA
Oc1ccc(c(c1)O)-c1csc(n1)Nc1ccccn1 	Z238766124	+	NA
COc1ccccc1Nc1nc(cs1)-c1ccc(o1)CNC(=O)C 	Z48856426	-	NA
CC(=O)NCc1ccc(o1)-c1csc(n1)Nc1cc(cc(c1)C)C 	Z48859481	-	NA
CC(=O)NCc1ccc(o1)-c1csc(n1)Nc1ccc(c(c1)Cl)F 	Z48857131	-	NA
COc1ccc(cc1)Nc1nc(cs1)-c1cc(n(c1C)-c1nnc[nH]1)C 	Z204017924	-	NA
Cc1cc(c(n1-c1nnc[nH]1)C)-c1csc(n1)Nc1ccccc1 	Z204003168	-	NA
CN1C(=C(C(=O)N(C)C1=O)c1csc(n1)Nc1ccc(cc1)F)N 	Z118606410	-	NA

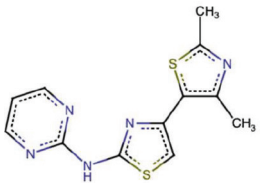
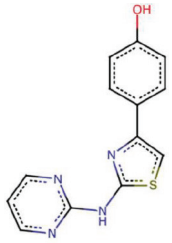
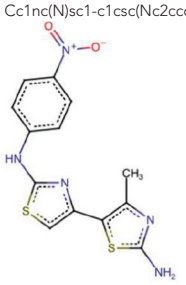
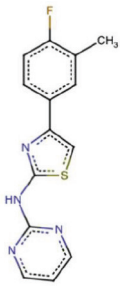
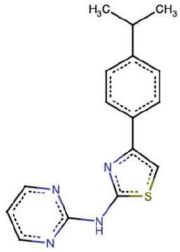
Continued on next page

Continued

Structure of compound 20 analogue and fragment	ID	ISR activation	GCN2 specificity
CN1C(=C(C(=O)N(C)C1=O)c1csc(n1)Nc1ccccc1)N 	Z94733799	-	NA
Br.CC(=O)Nc1nc(c(s1)-c1csc(n1)Nc1ccccc1)C 	Z2854692688	-	NA
Br.CC(=O)Nc1nc(c(s1)-c1csc(n1)Nc1ccccn1)C 	Z2239043599	-	NA
Cc1cc(c(n1CC(F)(F)F)C)-c1csc(n1)Nc1ccccn1 	Z238766162	+	NA
Cl.Cc1cc(c([nH]1)C)-c1csc(n1)Nc1ccccn1 	Z381026350	-	NA
Cl.Cc1cc(c(n1C1CC1)C)-c1csc(n1)Nc1ccccn1 	Z357935644	-	NA
Cl.Cc1cc(c(n1C)C)-c1csc(n1)Nc1ccccn1 	Z381543540	-	NA
Cc1nccc(n1)NCCCc1nc(cs1)-c1ccccn1 	Z2582963583	-	NA

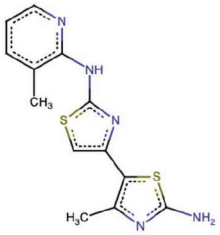
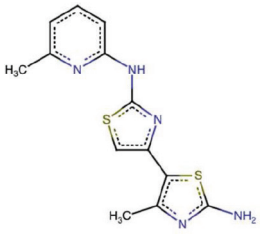
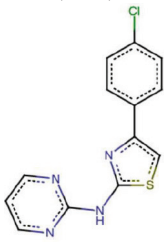
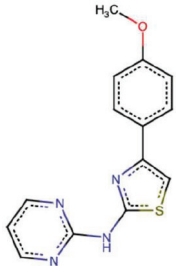
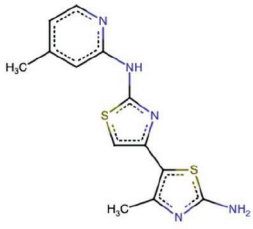
Continued on next page

Continued

Structure of compound 20 analogue and fragment	ID	ISR activation	GCN2 specificity
Cc1nc(C)c(-c2csc(Nc3ncccn3)n2)s1 	BCC0083926	-	NA
Oc1ccc(-c2csc(Nc3ncccn3)n2)cc1 	BCC0089540	+	+
Cc1nc(N)sc1-c1csc(Nc2ccc([N+](=O)[O-])cc2)n1 	BCC0084097	++	-
Cc1cc(-c2csc(Nc3ncccn3)n2)ccc1F 	BCC0080200	-	NA
CC(C)c1ccc(-c2csc(Nc3ncccn3)n2)cc1 	BCC0080152	-	NA

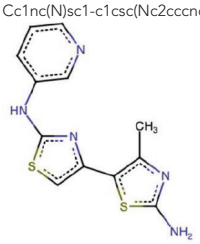
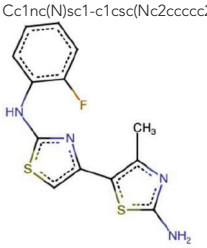
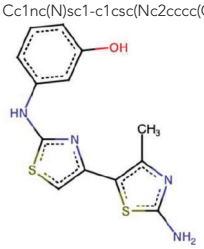
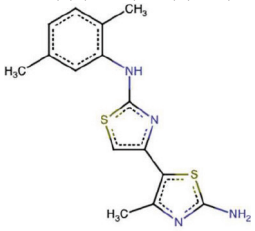
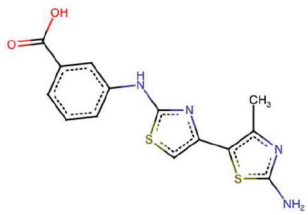
Continued on next page

Continued

Structure of compound 20 analogue and fragment	ID	ISR activation	GCN2 specificity
Cc1cccnc1Nc1nc(-c2sc(N)nc2C)cs1 	BCC0084738	+	+
Cc1cccc(Nc2nc(-c3sc(N)nc3C)cs2)n1 	BCC0084842	-	NA
Clc1ccc(-c2csc(Nc3ncccn3)n2)cc1 	BCC0075509	-	NA
COc1ccc(-c2csc(Nc3ncccn3)n2)cc1 	BCC0057431	-	NA
Cc1ccnc(Nc2nc(-c3sc(N)nc3C)cs2)c1 	BCC0083923	+	+

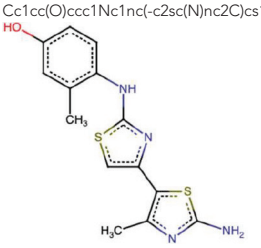
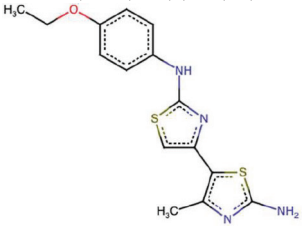
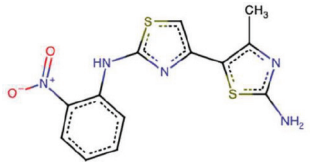
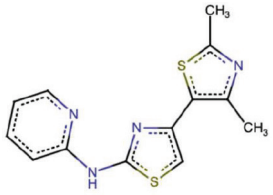
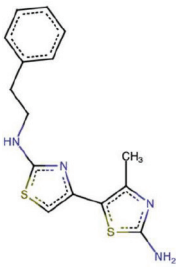
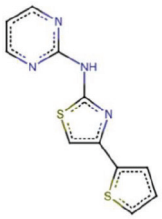
Continued on next page

Continued

Structure of compound 20 analogue and fragment	ID	ISR activation	GCN2 specificity
Cc1nc(N)sc1-c1csc(Nc2cccnc2)n1 	BCC0084758	-	NA
Cc1nc(N)sc1-c1csc(Nc2ccccc2F)n1 	BCC0084762	+	-
Cc1nc(N)sc1-c1csc(Nc2cccc(O)c2)n1 	BCC0105427	-	NA
Cc1ccc(C)c(Nc2nc(-c3sc(N)nc3C)cs2)c1 	BCC0084833	-	NA
Cc1nc(N)sc1-c1csc(Nc2cccc(C(=O)O)c2)n1 	BCC0057014	-	NA

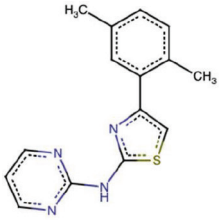
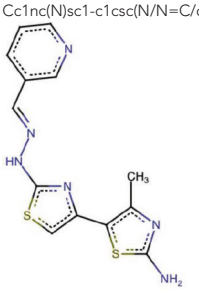
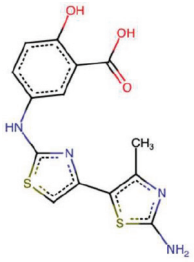
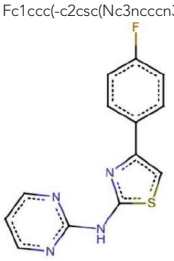
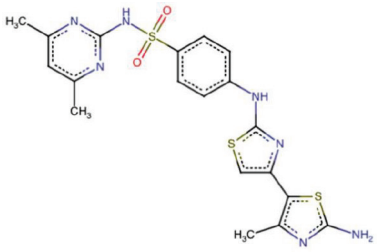
Continued on next page

Continued

Structure of compound 20 analogue and fragment	ID	ISR activation	GCN2 specificity
Cc1cc(O)ccc1Nc1nc(-c2sc(N)nc2C)cs1 	BCC0084814	-	NA
CCOc1ccc(Nc2nc(-c3sc(N)nc3C)cs2)cc1 	BCC0087543	+	-
Cc1nc(N)sc1-c1csc(Nc2ccccc2[N+](=O)[O-])n1 	BCC0084744	-	NA
Cc1nc(C)c(-c2csc(Nc3ccccn3)n2)s1 	BCC0079350	++	-
Cc1nc(N)sc1-c1csc(NCCc2ccccc2)n1 	BCC0089615	-	NA
c1cnc(Nc2nc(-c3cccs3)cs2)nc1 	BCC0079876	-	NA

Continued on next page

Continued

Structure of compound 20 analogue and fragment	ID	ISR activation	GCN2 specificity
Cc1ccc(C)c(-c2csc(Nc3ncccn3)n2)c1 	BCC0080199	-	NA
Cc1nc(N)sc1-c1csc(N/N=C/c2cccnc2)n1 	BCC0041121	-	NA
Cc1nc(N)sc1-c1csc(Nc2ccc(O)c(C(=O)O)c2)n1 	BCC0089519	-	NA
Fc1ccc(-c2csc(Nc3ncccn3)n2)cc1 	BCC0084830	-	NA
Cc1cc(C)nc(NS(=O)(=O)c2ccc(Nc3nc(-c4sc(N)nc4C)cs3)cc2)n1 	BCC0087668	-	NA

NA = not applicable; assay not performed due to the inactivity of the analogue or fragment.